International Journal of Heat and Mass Transfer 109 (2017) 40–62

Contents lists available at ScienceDirect

International Journal of Heat and Mass Transfer

journal homepage: www.elsevier.com/locate/ijhmt

Vortex heat transfer enhancement in the narrow plane-parallel channel with the oval-trench dimple of fixed depth and spot area

S.A. Isaev [a,c,*], A.V. Schelchkov [a], A.I. Leontiev [b], Yu F. Gortyshov [a], P.A. Baranov [c], I.A. Popov [a]

[a] Tupolev Kazan National Research Technical University – Kazan Aviation Institute, Kazan, Tatarstan, Russia
[b] Bauman Moscow State Technical University, Moscow, Russia
[c] Saint-Petersburg State University of Civil Aviation, Saint-Petersburg, Russia

ARTICLE INFO

Article history:
Received 4 December 2016
Received in revised form 27 January 2017
Accepted 27 January 2017

Keywords:
Turbulent heat transfer
Hydraulic losses
Narrow channel
Spherical, conical, oval, oval-trench dimples
Reynolds-Averaged Navier-Stokes (RANS) equations
Multiblock computational technologies

ABSTRACT

The article is devoted to the analysis of vortex heat transfer enhancement due to the use of oval-trench dimples. The main role in the understanding of this process is associated with the application of the technologies developed in engineering practice thanks to design decisions. As a result, prevailing interest has been paid to a spherical dimple when a spot diameter is chosen as a characteristic size, whereas hydraulic losses depend on the dimple-to-device size ratio. Progress in vortex heat transfer enhancement due to the use of oval dimples is connected with the explanation of the mechanism of generation of both vortex structures in dimples and spiral vortices behind them. An abrupt increase of heat transfer in the vicinity of the spherical dimple due to the restructuring of the flow structure in the dimple with two vortices to that in the dimple with one spiral vortex made it possible to propose a new shape of a surface vortex generator – an oval dimple located at an angle of inclination to the incoming flow and consisting of two spherical dimple halves separated by a cylindrical insert. The generation of vortex structure in this case is rather stable and intense in comparison to spherical dimple. The numerical results for vortex heat transfer enhancement in the turbulent water flow in the rectangular narrow channel with spherical, 10°-truncated conical and oval dimples of the same spot area and depth at the heated wall are presented. In the article, central attention is given to the mechanism of secondary flow restructuring and heat transfer enhancement due to increase in a relative length and width of an oval dimple followed by the formation of a long spiral vortex in it. The change in the length of the oval dimple (in terms of its width) from 1 to 6.78 allowed one to rationally mount spiral vortex surface generators in the narrow channel with high thermal and thermal-hydraulic efficiencies, significantly exceeding the identical characteristics of channels with spherical and conical dimples. In this case, moderate hydraulic losses in the channel with an oval-trench dimple, when its length is increased to 6.78, are comparable to those in the channel with a basic spherical dimple.

1. Introduction

The topic of heat and mass transfer enhancement due to surface vortex generators – dimples in a remarkable way combines the fundamental and applied aspects of research. Growing interest to this topic is primarily the result of achieving the effect of increasing heat output coefficient at low (as compared to surface protrusions) hydraulic losses. Moreover, it features a wide range of practical applications characterized by a variety of scales (from micro to macro), flow regimes, geometric shapes, and determining sizes of objects under study. Of extreme importance for this topic is the technology of making dimples that in fact predetermine the selection of simple-topology cavities in effort to investigate geometric shapes. Not by chance, the overwhelming majority (more than 90%) of the publications is devoted to heat transfer enhancement due to spherical dimples. The fundamental aspect of vortex heat transfer enhancement is also connected with the fact that it serves as a polygon both for testing the developed and modified semi-empirical turbulence models and for developing the efficient methods of numerical simulation. Over several decades of solution of the dimple problem the way has been passed from industrial design to complex aero-thermophysical design of surface reliefs with the implication of the principles of organization of vortex structures. It has appeared that spherical dimples are not high-performance vortex generators since maximum secondary flow velocities generated by them do not exceed 30–40% of the bulk

* Corresponding author at: Saint-Petersburg State University of Civil Aviation, Saint-Petersburg, Russia.

http://dx.doi.org/10.1016/j.ijheatmasstransfer.2017.01.103
0017-9310/

Nomenclature

b	width of an oval dimple, in terms of spot diameter d
C_p	pressure coefficient, $C_p = 2(P - P_{ref})/\rho U^2$
C_c, C_μ	semi-empirical constants
c_p	heat capacity
d	spot diameter of a spherical dimple (m)
f	friction, $f = \tau_w/\rho U^2$
f_μ	correction function
h	height of a narrow channel, in terms of d
L	cylindrical insert lengthening of an oval dimple, in terms of d
k	kinetic turbulence energy based on U^2
Nu	Nusselt number, $Nu = \alpha d/\lambda$
Nu_s	Nusselt number integrated over the dimple region
P	pressure (N m^{-2})
p	pressure based on ρU^2
Pr	Prandtl number, $Pr = \mu c_p/\lambda$
q	dimensionless surface heat flux
$\dot{q}$	surface heat flux (W m^{-2})
Re	Reynolds number, $Re = \rho U d/\mu$
Ri_t	turbulent Richardson number
s	coordinate along the longitudinal middle cross section of an oval dimple, in terms of d
T	temperature, in terms of 293 K
t	coordinate along the transverse middle cross section of an oval dimple, in terms of d
THE	thermal hydraulic efficiency
U	bulk velocity (m/s)
u, v, w	longitudinal, vertical, and transverse velocity components, in terms of velocity U
$\vec{V}$	local velocity vector, in terms of U
x, y, z	longitudinal, vertical, and transverse coordinates, in terms of d
$\vec{x}$	radius-vector

Greek symbols

α	heat transfer coefficient based on the spot area, $\dot{q}/(T_w - T_{bulk})$ (W m^{-2} K^{-1})
Δ	dimple depth, in terms of d
ζ	hydraulic loss coefficient
λ	thermal conductivity (W m^{-1} K^{-1})
μ	dynamic viscosity coefficient (kg/(m s))
ν	kinematic viscosity coefficient, in terms of Ud
ξ	dependent variable
ρ	density (kg/m^3)
τ	stress (N m^{-2})
χ	oval dimple lengthening, in terms of width b
ω	specific dissipation rate, in terms of U/d

Subscripts

bulk	local bulk temperature
extr	extreme value
f	friction
m	quantity averaged over the wall section strip
min, *max*	minimum, maximum quantities
n	quantity averaged over the projection area of the dimpled section
n_o	quantity averaged over the area of the dimpled section
pl	plane wall
ref	reference value at the inlet
t	turbulent
w	local wall
‘	fluctuation characteristics
1	parameters determined over the 3×2 section with the dimple center at the distance of 1 from the front boundary of this section
2	parameters determined over the section surrounding the dimple

Abbreviations

AMG	algebraic multigrid accelerator
BiCGStab	biconjugate gradient stabilized method
ILU0	preconditioner
QUICK	quadratic upwind interpolation for convective kinematics
RANS	Reynolds-averaged Navier-Stokes equations
RLI	Rodi-Leschziner-Isaev
SIMPLEC	semi-implicit method for pressure-linked equations (convenient)
SST model	shear stress transfer model
TVD	total variation diminishing
VP2/3	velocity-pressure, 2D/3D version

velocity. This fact exerts an influence on an attainable heat output value on the windward side of the dimple and in its wake. Moreover, on the inner surface of the spherical dimple weak separated flow zones are characterized by decreased heat transfer in comparison to the plane wall. Therefore, to impart high thermal efficiency to reliefs, very densely packed spherical dimples have been used. As an alternative to spherical dimples, the following approach has been proposed, which was actively developed in effort to design asymmetric oval-trench dimples with a ‘spot area’ of oval shape. These dimples consist of two spherical dimple halves separated by a cylindrical insert. Dimples are located at an optimal angle of inclination of about 45° to the incoming flow in the narrow channel. The preliminary results have shown that oval dimples are capable of producing secondary flows with maximum local velocities of about 80% of the characteristic bulk velocity in the channel. This permits one to consider them as high-performance vortex generators for heat transfer enhancement. This work analyzes the results of vortex heat transfer enhancement and the choice of a rational shape of an oval dimple located at the heated (q = const) wall of the narrow channel. Terekhov’s experimental setup is chosen as a test facility. It is a 2×0.33 rectangular channel, whose wall is provided with oval dimples having a different-length insert and a fixed ‘spot’ area, as in the case both of the basic spherical dimple (the spot diameter is equal to 1) and of the 10°-truncated conical dimple, whose shape is close to cylindrical, at a depth of 0.13 (in terms of ‘spot’ area diameter). The lengthening of the oval dimple is varied from 1 to 6.78 in terms of its width. The Reynolds number defined through the spot diameter d of the spherical dimple and the water flow bulk velocity U is taken as equal to 10^4.

2. Heat transfer enhancement in channels with oval dimples

As known [1], one of the promising means to enhance heat transfer in power equipment plants, including in heat exchangers, is to organize discrete roughness on streamlined surfaces. However, when periodic protrusions are located, for example, at the channel wall, a considerable increase in heat output is accompanied by an advanced growth of hydraulic losses. Sometimes this requires that extreme total pressure drops be assigned. It has appeared possible to decrease hydraulic losses when protrusions have been replaced by depressions. It is of importance to note that

the discrete roughness relief at the wall was mainly predetermined by the technology of its making. The early studied cylindrical cavities formed by dimpling [2–4] were most ease to manufacture. However, the hydraulic losses, when heat carrier was flowing in the channel with such cavities, appeared to be very substantial. Another rather simple shape of a cavity was a hemispherical dimple made by pressing a sphere against a deformable wall. At first, the experimenters [5–8] paid attention to such cavities, although later they often considered segment-spherical dimples of a relative depth of less than 0.5 (in terms of spot diameter). For example, the self-oscillatory regime [5] was revealed in the cavity where vortices were alternately formed on its sides.

An important contribution to the understanding of the physical mechanisms of vortex heat transfer enhancement on reliefs with spherical dimples was made by Kiknadze, who proposed the concept of self-organizing vortex flows [9] for dimples with smoothed edges, and by Ligrani [10]. Works [11,12] should be mentioned among the pioneer experimental studies of turbulent convective heat transfer at the plane wall with shallow spherical dimples, both single and in ensembles, in particular in the narrow channel. Also, the retrospective analysis of the available works was based on Terekhov's fundamental publication [13] combining the traditional methods for pressure and heat load determination and the laser Doppler measurements of mean and fluctuation velocities in the narrow channel with a single dimple. Ten years later, the results of this work were used as a prototype for investigation of flow characteristics in the narrow channel with spherical dimples in Rostock (Germany) [14].

A large series of experimental works on vortex dynamics and heat transfer on dimpled reliefs was carried out at the beginning of the century [15–20]. Later, these works were supplemented [21–23]. Here, it should be noted that heat flux gradient sensors and original pressure pulsation detectors found use.

Computational studies of spherical dimples started in the early 90s of the last century. First of all, the works based on solving the Reynolds-averaged Navier-Stokes equations closed by the two-parameter dissipative turbulence model should be mentioned. The interesting 'vacuum cleaner effect', when a medium is being pumped from the surrounding into the shallow dimple region [24], was revealed. The patterns of separated flow around single dimples on the surface with increasing Reynolds number [25–32] were obtained. Dimples and trenches were compared [33]. Heat transfer enhancement in channels with single spherical dimples was examined [34–40] and was influenced by restructuring the structure with a symmetric vortex to that with a spiral vortex. Flow of heat carrier (air, water, oil) and heat transfer in channels with a set of spherical dimples located at the wall were numerically simulated [41–48]; in a number of works, the Fluent code with unfounded boundary conditions (unjustified symmetry conditions at the side boundaries of the computational domain) was applied. Much attention was given to the numerical simulation of turbulence within the framework of the LES/DNS approaches [49–51].

The subject matter of this study focuses on finding a rational shape of dimples, especially asymmetric ones. Retrospectively, work [52] dealing with a set of conical dimples at the walls of converging and diverging channels should be mentioned. Work [53] analyzed the dimples having a different shape of a spot. An attempt was made to optimize the dimple shape using the experiment planning methods [54] and the genetic optimization algorithms were applied [14]. Also, it was advisable to organize some bulge at the bottom of the spherical dimple. Unfortunately, the cited works did not use the flow control concept for determining a rational shape of a dimple, namely: for designing a streamlined contour of a dimple with regard to the formation of a preferable vortex flow structure in it.

The growth of heat transfer from the wall is largely caused by increase in the secondary flow intensity in the near-wall region. One of the pioneer works on numerical simulation [55] attempted at realizing asymmetric flow around the spherical dimple. To do this, a short splitter was placed on its side to prevent a medium flow into the interior of the dimple with a low-pressure zone developing in it. Later, the idea appeared to vary the rounding off radius of an edge by changing the circumferential coordinate, as well as by connecting the side half of the elliptical dimple with that of the spherical dimple [56].

However, the concept of a surface spiral vortex generator recessed into the wall – the analog of the vane-type protrusion shaped as an oval dimple consisting of two spherical dimple halves connected by a cylindrical insert proved to be more effective. Such a dimple can be turned at an inclination angle relative to the incoming flow. Emphasis is made both on the intense vortex structure forming in the dimple and on the vortex flow in the dimple wake. If in the large-depth spherical dimple, the periodic flow regime is realized when vortex structures are transported left to right and right to left [14], then the oval dimple generates a spiral vortex of stable orientation. The first experiment-calculated study was made in [57] and continued in [58–64].

These works revealed that oval dimples are preferable in thermal efficiency as compared to spherical ones, especially in strongly viscous media. However, most works considered oval dimples of moderate lengthening (about 2–3 in terms of width). In addition, it was not taken into account that different dimple shapes should have been compared under the condition of a fixed spot area. The present work, as well as work [64] is dealing with oval dimples of relatively large lengthening (up to approx. 7 in terms of width). Of special interest is the analysis of the influence of increase in the relative lengthening of the dimple on the restructuring mechanism of the vortex structure forming in it, as well as on the enhancement of secondary flow and heat transfer. The computer model of the narrow channel, whose heated wall is provided with an oval dimple of variable lengthening at a fixed depth (0.13) and a fixed spot area at $Re = 10^4$, corresponds to the test facility in Terekhov's experimental setup [13]. Numerical simulation of convective heat transfer in the dimpled channel is made, as is done in [38,40] when the boundary condition of the wall temperature $T = \text{const}$ is replaced by that of the heat flux $q = \text{const}$ and when air hear carrier is replaced by water one. The basic spherical and 10°-truncated conical dimples of the same spot area and depth are compared in detail.

3. Problem statement, models, methods, computational grids

Convective heat transfer is studied in the 2.5×0.33 rectangular narrow (in terms of spherical dimple diameter) channel, at whose inlet the velocity profile of a fully developed turbulent flow of incompressible liquid is assigned. No-slip conditions are satisfied at the streamlined walls. The profiles of the longitudinal, vertical, and transverse velocity components u, v, w, as well as the turbulence characteristics (energy k, specific dissipation rate ω, vortex viscosity μ_t) are defined when solving a special task about the flow in the periodic section of the considered channel at the Reynolds number equal to 10^4. The bulk velocity U, the spot diameter d of the basic spherical and 10°-truncated conical dimples, the density ρ, and the viscosity μ of heat carrier – water ($Pr = 7$) are assigned as dimensionalization scales. Dimples of the moderate (according to the classification [38]) depth equal to 0.13 are located at some distance (about 3) from the channel inlet taken under the provision of their insignificant influence on the inlet conditions. The center of the Cartesian (x, y, z) coordinate system is in the longitudinal middle plane of the channel at the point of the dimple center projec-

tion onto the section coinciding with the bottom plane wall (Fig. 1). The rounding off radius of the dimple edge is taken as equal to 0.025. When the spot area of the oval dimple is kept equal to that of the basic spherical dimple, its width b is varied from 0.731 to 0.346 and the dimple length based on the width – from 1.68 to 6.78 (Fig. 1 and Table 1).

Outflow boundary conditions are assigned at the channel outlet of length 7.

The heat task is being solved separately from the fluid dynamics one (natural convection effects are not taken into consideration). At the channel inlet the flow is isothermal and has $T_{ref} = 293$ K. The streamlined bottom wall of the dimpled channel is heated and the supplied constant heat flux q is re-calculated in dimensionless form by the formula

$$q = \dot{q}/[\lambda\ Pr\ Re\ T_{ref}/d] \text{ (of the order of } 3.4 \cdot 10^{-5}).$$

Here, λ is the thermal conductivity of water. The side walls of the channel are adiabatic and the top wall is isothermal and has T_{ref} taken as the dimensionalization scale. The outflow boundary conditions are predetermined for T at the channel outlet.

Table 1
The cylindrical insert length, the width of oval dimple and its relative lengthening in width fractions.

L	b	χ
0.5	0.731	1.68
0.625	0.678	1.92
0.675	0.659	2.02
0.75	0.631	2.19
0.9	0.58	2.55
1	0.549	2.82
1.25	0.482	3.59
1.5	0.429	4.50
1.75	0.383	5.57
2	0.346	6.78

3.1. Turbulence models

As in [38,40], to solve the problem on convective heat transfer in the 3D steady-state fully turbulent flow of incompressible liquid in the plane-parallel channel with a single dimple at the heated wall, the mathematical model based on the system of the Reynolds-averaged steady-state Navier-Stokes (RANS) equations and the energy equation is used.

For these equations to be closed, the shear stress transfer (SST) model (2003) [65] modified with the consideration of the streamline curvature within the Rodi-Leschziner-Isaev (RLI) approach was adopted. As most semi-empirical models of differential type, this model includes the tensor module of strain rates S in the expression for vortex viscosity. It is of significance to emphasize that the semi-empirical models are mainly verified through near-wall flows; as a result, there is a need to verify them through separated flows with high rate. The Rodi-Leschziner-Isaev (RLI) approach for vortex viscosity correction means that the vortex viscosity is affected by the correction function $f_\mu = 1/(1 + C_c \times Ri_t)$; the constant $C_c = 0.02$ [66] is taken from the condition for the best agreement between numerical predictions and experimental data for numerous examples of separated flows. Here, $Ri_t = \left(\frac{1}{C_\mu \omega}\right)^2 (\nabla \times \vec{V}) \cdot \left(\frac{\vec{V}}{|\vec{V}|} \times \left(\frac{\partial \vec{V}}{\partial \vec{x}} \cdot \frac{\vec{V}}{|\vec{V}|}\right)\right)$ is the turbulent Richardson number. The correction value is within the range $0.02/C_\mu < f_\mu < 0.15/C_\mu$ where $C_\mu = 0.09$ [14,24].

3.2. Methodology of calculations

There is no doubt that the application program packages based on the solution of the Reynolds-averaged Navier-Stokes equations

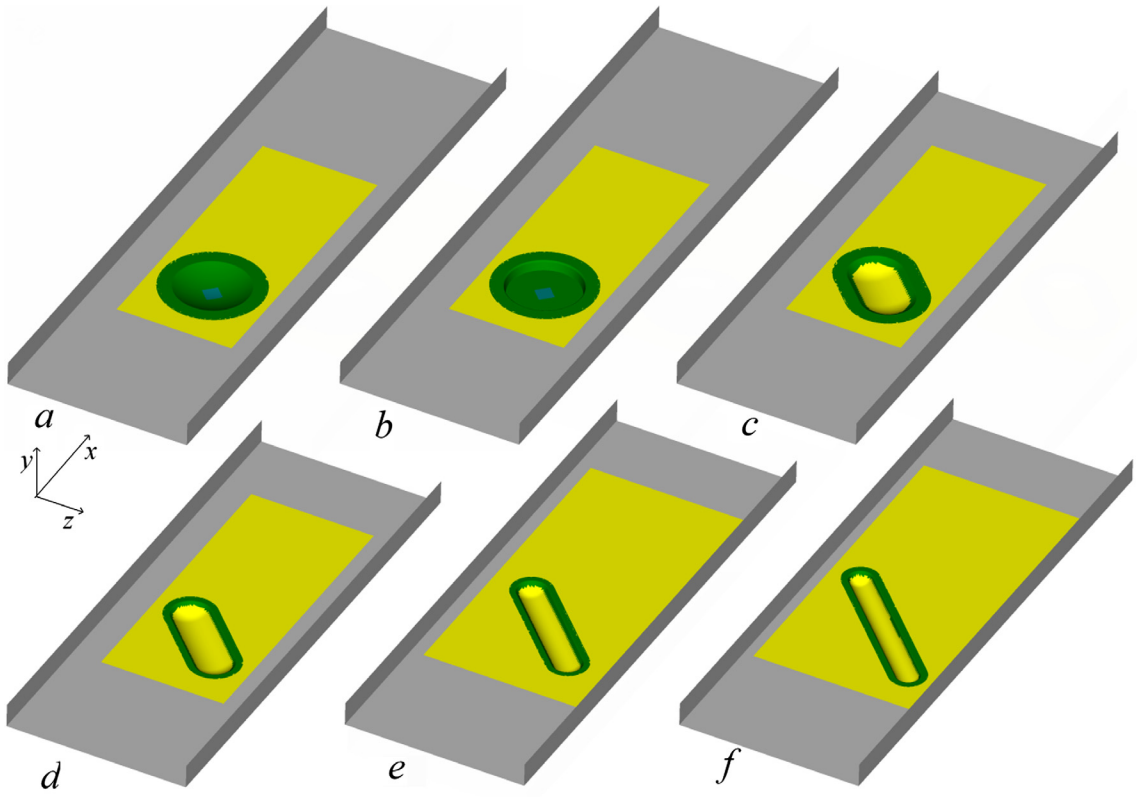

Fig. 1. Narrow channels with spherical (a), 10°-truncated conical (b) and oval dimples of width b = 0.731 (c), 0.549 (d), 0.429 (e), and 0.346 (f).

with the implication of the catalog of semi-empirical models have become a powerful tool to predict flow parameters and turbulence characteristics. The present study uses the multiblock computational technologies [67] realized in the original research VP2/3 code (velocity-pressure, 2D/3D). The computational algorithms realized in this code are based on the concept of splitting into physical processes and on the application of grid methods for solution of the governing equations.

The use of the concept of splitting into physical processes allows the system of partial differential equations to be divided into blocks containing the momentum equations in natural variables (including Cartesian velocity components for incompressible viscous liquid flows), the pressure correction equation (SIMPLEC [68]) replacing the continuity equation, as well as the equations for their closure (from the chosen turbulence model).

The system of stationary equations in discrete form is thus being solved block by block at each time step during the global iteration process (about 10–20 iterations), when at each time step for one iteration in the course of solution of the momentum equation, several (about 10–15) iterations are being performed in the pressure correction block and about 4–6 iterations – in the turbulence and energy blocks.

The specific features of the used algorithm are: (1) based on the concept of splitting into physical processes, the pressure correction procedure SIMPLEC [68] together with Rhie-Chow's monotone approximation for a given centered computational block [69,70]; (2) the approximation of the convective terms in the explicit hand-side of the momentum equation by the one-dimensional analog of Leonard's quadratic upwind scheme [71] to reduce the influence of numerical diffusion specific for the considered type of separated flows and by Van Leer's scheme [72] for the equations of turbulence and energy characteristics; (3) the representation of the convective terms in the implicit hand-side of the transport equation by means of the upwind scheme with one-sided differences, which allows the stability of the computational procedure to be improved; and (4) the application of methods with preconditioners for solution of difference equations [73].

The method for solution of algebraic equations is the preconditioned BiCGStab containing the AMG preconditioner taken from Demidov's library (amgl) [74] for pressure correction and the ILU0 preconditioner for another variables.

The multiblock computational technologies realized in the VP2/3 code are outlined elsewhere in [67,75]. The essence of these technologies lies in introducing a set of difference-scale, tier, and structured overlapping grids around solvable structural elements of the physical problem of relevant scales. In the two rows of the near-boundary cells of each of the overlapping or overset grids, the parameters are determined through the linear interpolation [67,76] in the manner, as done in [77]. The use of this approach is more effective since it is based on the application of adaptive unstructured grids and it requires less computational resources. This approach also provides a proper computational accuracy without refining grids since it automatically resolves the identified structural features of flow.

Computation from grid to grid with the use of the multiblock computational technologies involving linear interpolation is a

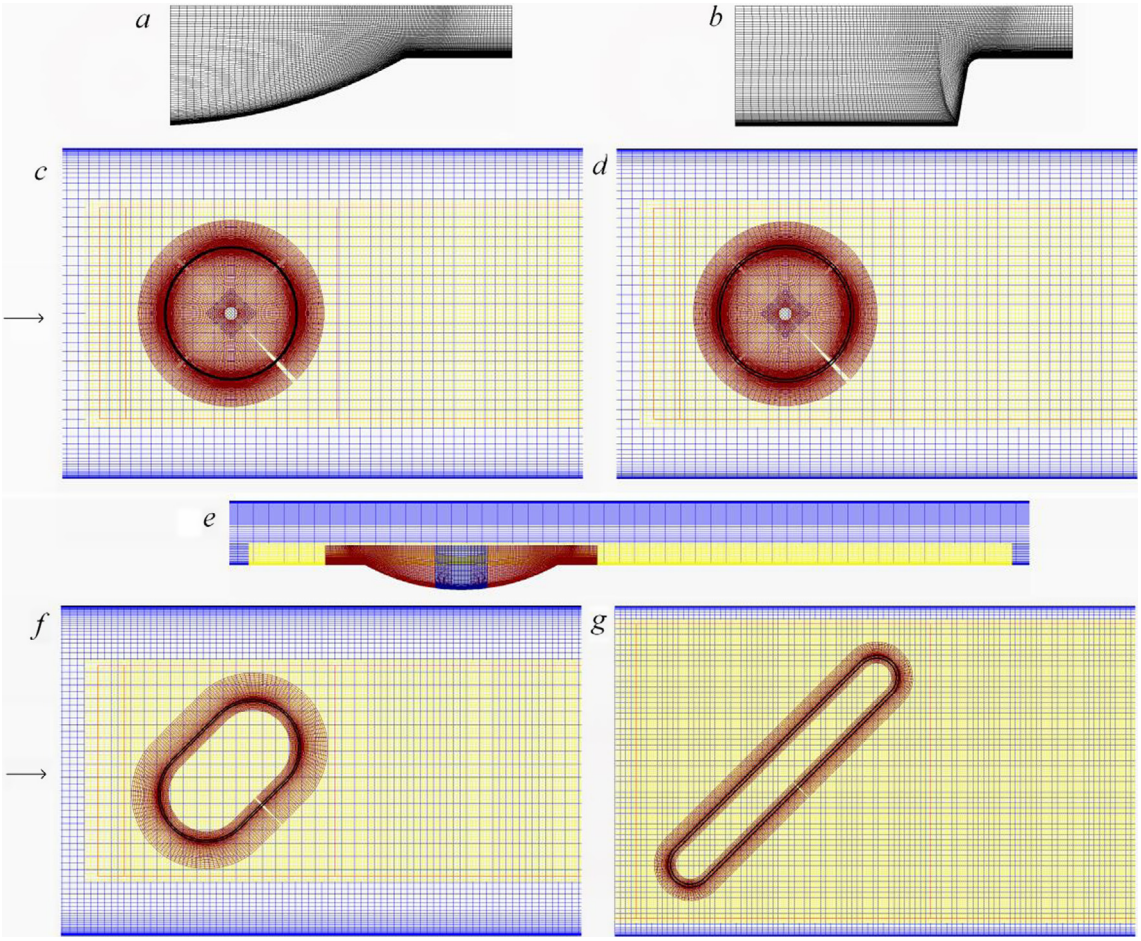

Fig. 2. Asymmetric spherical (a) and 10°-truncated (b) inserts into multiblock structured grids in the narrow channel with single spherical (c and e), conical (d) and oval (f and g) dimples of different topology and width: c, d, f,g – view from the heated wall side; e – middle cross section of the channel; f – b = 0.731; g – 0.346.

source of errors; however, the test calculations of steady circulation flow in the cavity with a moving cover [76] showed that the error values are quite acceptable.

3.3. Computational grids

The present study deals with solving the tasks about vortex enhancement of convective heat transfer in the narrow channel having a single dimple with the use of multiblock overlapping structured grids of different scale (Fig. 2). The grid structures similar in topology to those used in [38,40] are considered, but are densely packed and have a large number of cells. A rectangular channel is covered with a Cartesian grid densely packed to the wall (the grid step is varied from 10^{-5} to 10^{-4}) and to the dimple (the minimum value of longitudinal and transverse grid steps is ranged from 0.04 to 0.08). The total number of cells in the channel is 700,000–1,500,000. Near the dimple there is a detailed, close to uniform, grid meant for resolving the structural features of flow in the near wake (the minimum grid step along and across the flow is varied from 0.015 to 0.03 in different variants). The height of the sub-domain with a detailed grid is 0.13 and the width is varied from 1.6 to 2.1 depending on the dimple size. The length of the sub-domain is about 3.

In the case of spherical and conical dimples, the detailed grid is Cartesian; in the case of oval dimples, it is curvilinear and matched with the streamlined bottom wall of the channel.

The area around spherical and conical dimples is divided by the cylindrical grid matched with the channel wall (Fig. 2a and b); to prevent the density of nodes in the near-axis zone, the additional grid close to the rectangular one ('patch') is introduced. The minimal grid step near the edge is 0.002. For oval dimples, a special edge grid is introduced to describe high-gradient zones of determining parameters.

The total number of multiblock grid cells is about 1.5–3 mln cells.

Fig. 3a illustrates the multiblock computational grid in the axonometric projection for an oval-trench dimple. The color shows the channel grid having rather coarse cells and covering the dimple

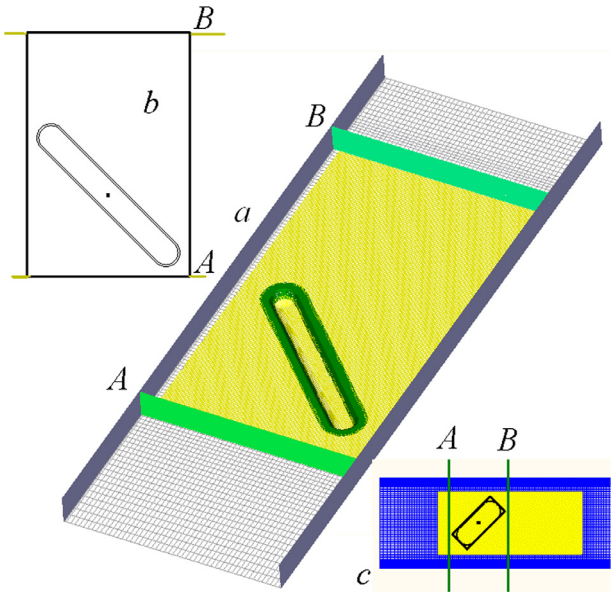

Fig. 3. Multiblock grid for the narrow channel with the oval-trench dimple involving a dimple with a detailed grid in the dimple region and the selection of edge grid (a), 3 × 2 section with a dimple (b) and the rectangle-selected vicinity of the oval dimple (c). The channel cross sections A–B serve for determination of hydraulic losses.

with a refined detailed grid in order to reflect both the curvilinear surface of the dimple itself and in detail vortex flow and heat transfer in the dimple wake, as well as the near-edge grid to resolve flow and heat transfer characteristics in high-gradient zones.

3.4. Data processing

The integral characteristics of flow and heat transfer in the narrow channel with single dimples are calculated using the selected channel sections surrounding the dimple. As in [38,40], the hydraulic losses in the channel were determined between assigned cross sections *A–B* in Fig. 3. Since oval-trench dimples were analyzed, it was necessary to increase the sizes of the channel section (in comparison to [35,38,40]) in order to assess relative heat transfer and to take them equal to 3 × 2 for the dimple center at the distance of 1 from the front boundary of the channel section (Fig. 3b). In the present work, the thermal efficiency of the oval dimple was for the first time determined over the channel rectangular section surrounding the dimple at an angle of inclination of 45° (Fig. 3c).

Local dimensionless and relative characteristics of flow and heat transfer, including static pressure, friction, temperature, and Nusselt number, are analyzed as the functions of longitudinal and transverse coordinates over the middle cross sections of the channel and the dimple at the bottom, heated, and isothermal top wall. The Cartesian velocity components, turbulence energy, and the vortex viscosity normalized by the Reynolds number are compared as the profiles along the vertical coordinate in the dimple centers.

The fields of the wall temperature and the Nusselt number are supplemented by the streamlines. Vortex structures formed in dimples, obtained by computer visualization with the use of the observation method of labeled liquid particles, are also considered.

4. Results and discussion

In the present study, main attention is focused on assessing the influence of oval dimple lengthening on fluid dynamics and heat transfer in the narrow channel with a dimple of fixed spot area, as well as on comparing the oval dimples having conical depressions with spherical and conical dimples. The study has been aimed at choosing an oval dimple that will be best in thermal/thermal-hydraulic efficiency. The work done embodies the concept of flow control by vortices during the efficient generation of spiral vortices due to oval-trench dimples to enhance secondary flow in the channel.

Figs. 4–17 and Tables 2 and 3 contain some of the obtained results.

4.1. Pressure distribution

Fig. 4 analyzes the static pressure distributions over the middle longitudinal and transverse cross sections of the channel at the heated bottom wall with a single dimple and at the opposite plane wall. The zero static pressure is assigned at the channel inlet. As seen from Fig. 4a and c, the pressure in the dimpled channel decreases and generally obeys the law close to the linear one. In the vicinity of the dimple, the pressure drops are seen; they can be sufficiently substantial for large-width dimples. The first group of dimples (curves 1–3) is selected. Among them are a 10°-truncated conical dimple, a spherical dimple, and also an oval dimple of width $b = 0.731$. This group is characterized by maximum static pressure values on the windward side of the dimple that exceed those at the channel inlet. And last but not least, it is important to note quite significant minimum pressure values in the near wake, much exceeding those in the plane-parallel channel.

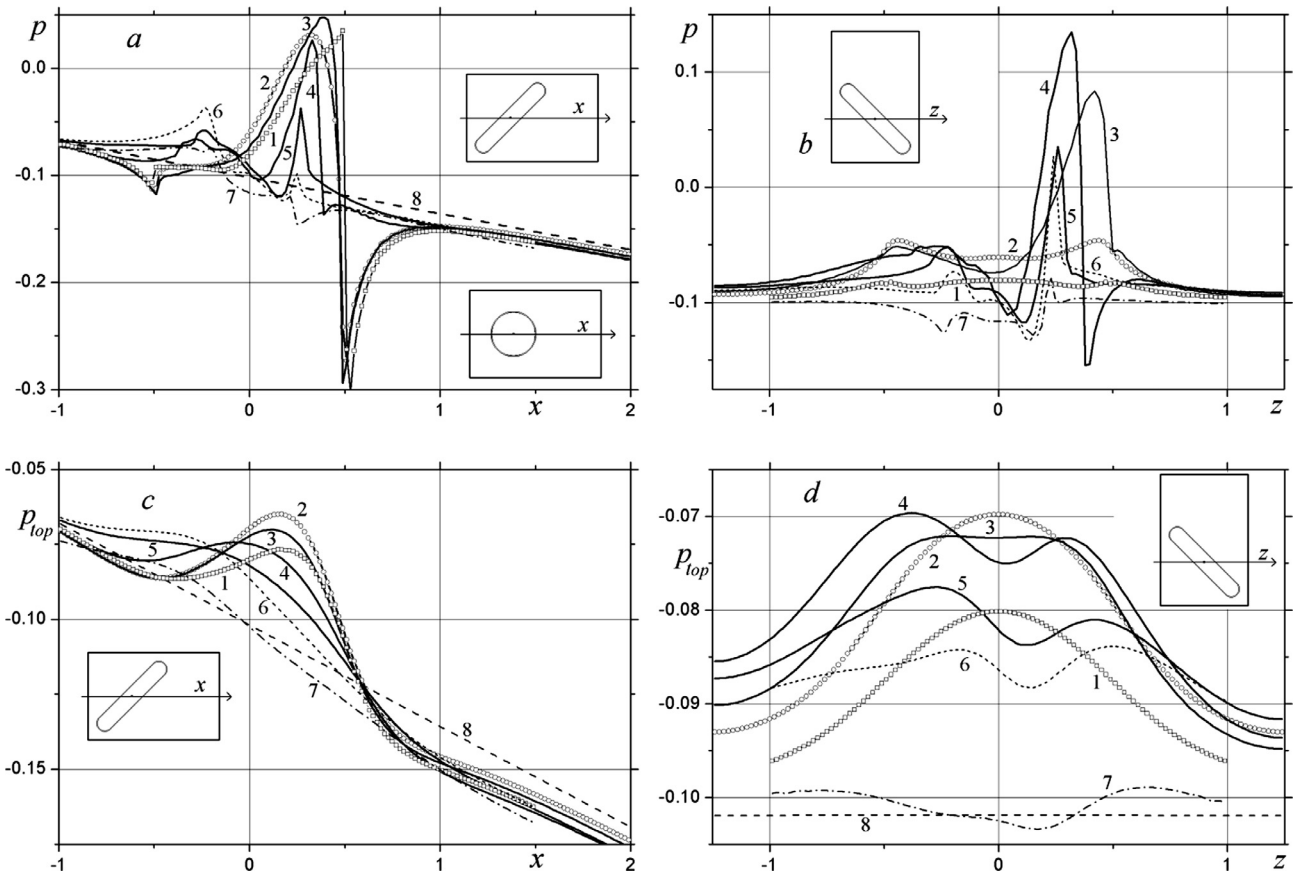

Fig. 4. Comparison of the dependences of static pressure over middle longitudinal (a and c) and transverse (b and d) cross sections of the channel at heated bottom (a and b) and isothermal top (c and d) walls for single conical (1), spherical (2) and oval (3–7) dimples of different width: 3 – b = 0.731; 4 – 0.549; 5 – 0.429; 6 – 0.383; 7 – 0.346. 8 – plane-parallel channel.

The oval dimple of width $b = 0.549$ with the cylindrical insert length $L = 1$ is intermediate between the oval dimples of small and large length (curve 4). It is characterized by increase in static pressure values in the dimple edge region on the windward side; however, there is no rarefaction behind the dimple edge. One more difference from the behavior of the pressure distribution of the first group of dimples is observed in the zone in front of the dimple. As seen from Fig. 4a, large-width dimples are characterized by the pressure drop in this zone, as compared to the pressure level in the plane-parallel channel. At the same time, on the contrary, for oval dimples the pressure increases in front of the dimple over its middle cross section.

The lengthening and the narrowing of the oval dimple are accompanied by decrease in maximum pressure values in the dimple edge region on the windward side; for the dimple of width $b = 0.346$, this process practically vanishes (curve 7). However, for the last dimple, the low-pressure zone again occurs behind it.

It is also of interest to note that the pressure in front of the oval dimple slightly grows at a width of 0.383 (curve 6) and then drops again at a width of 0.346 (curve 7).

Fig. 4b demonstrates the transverse static pressure distributions at the dimpled heated wall. The relatively smooth pressure distributions for symmetric dimples (curves 1 and 2) are strikingly different from the pressure distributions for oval dimples of moderate length and large width (curves 3, 4, and 5 are the cylindrical insert length equal to 0.5, 1, and 1.5, respectively). The above oval dimples are characterized by maximum pressure values in the edge region; the largest values are observed at the dimple width $b = 0.549$; with a further narrowing of the dimple, maximum pressure values decrease, almost vanishing at $b = 0.346$. It is of interest to note that at $b = 0.549$, a minimum local pressure value arises behind the trailing edge of the dimple and it is absent at another width of the oval dimple. As the width of the oval dimple is decreased and its length is increased, the maximum local static pressure value on its left (leading) edge gradually decreases, tending to the pressure value over the same cross section of the plane-parallel channel (curve 8 in Fig. 4d). The pressure on the inner surface of the dimple also decreases as the width of the dimple is decreased and its length is increased.

Over the dimple middle cross section at the smooth top wall of the channel above the dimple, the local pressure (Fig. 4c) has a maximum value that is greatest for the spherical dimple. As mentioned, curves 1–3 for the first group of dimples are pretty close. As the width of the oval dimple is decreased and its length is increased, the maximum pressure value decreases and is seen upstream.

The transverse pressure distributions over the middle cross section of the isothermal top wall for the first group of dimples: conical and spherical dimples, and the oval dimple of moderate lengthening are symmetric, although over the oval dimple of width $b = 0.731$ the pressure attains a constant value; it is of interest to emphasize that maximum pressure values for spherical and oval dimples are pretty close and are much larger than those for the conical dimple. The remaining oval dimples are characterized by the two-mode pressure distribution; as the dimple width is decreased, the pressure value decreases and at $b = 0.346$, the pressure value at the top wall is close to that in the plane-parallel channel.

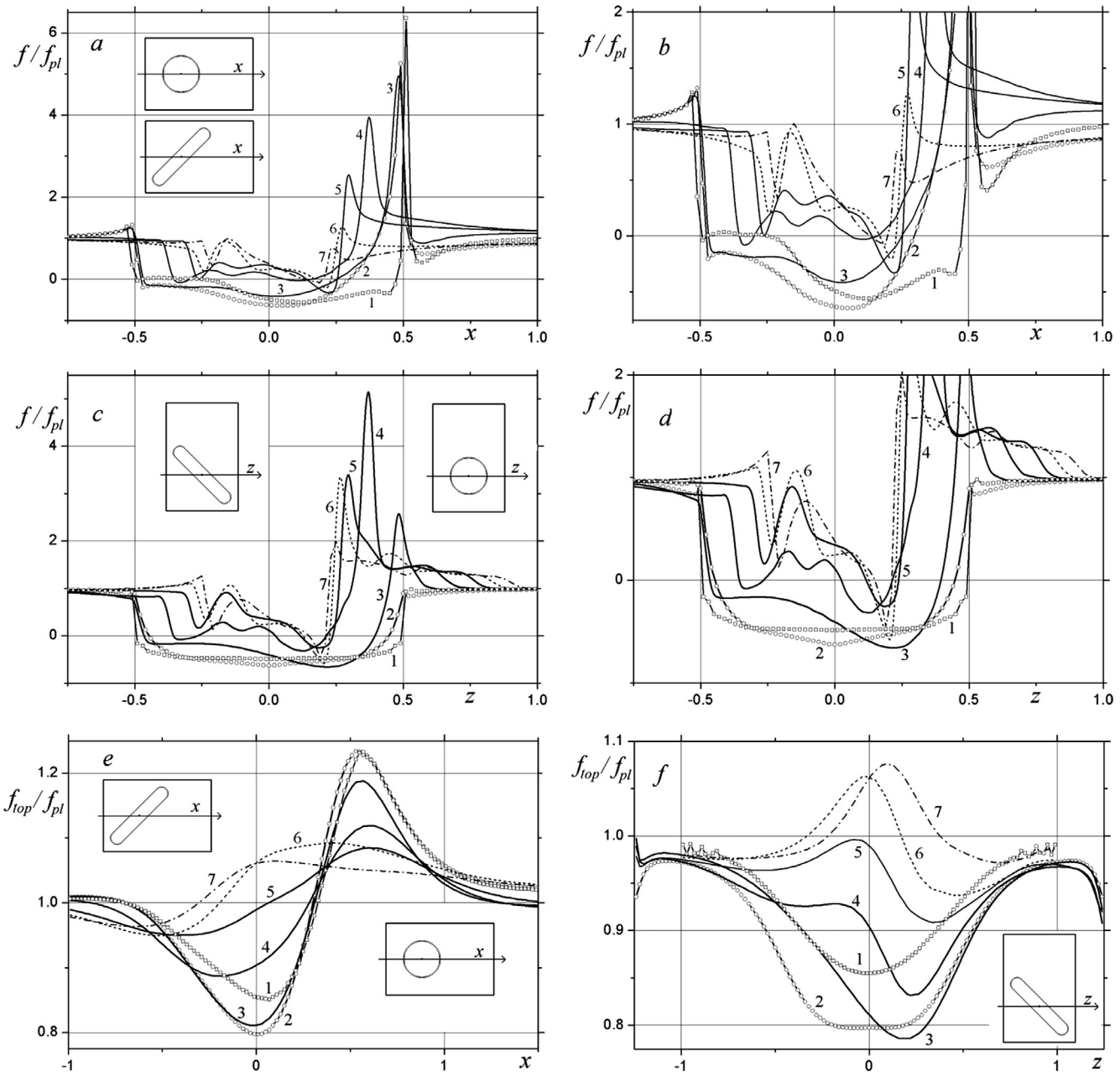

Fig. 5. Comparison of the dependences of relative friction over middle longitudinal (a, b, and e) and transverse (c, d, and f) cross sections of the channel at heated bottom (a–d) and isothermal top (e and f) walls for single conical (1), spherical (2) and oval (3–7) dimples of different width: 3 – b = 0.731; 4 – 0.549; 5 – 0.429; 6 – 0.383; 7 – 0.346. b and d – fragments of the dependences in enlarged scale.

4.2. Friction

Figs. 5 and 6a and b analyze the distributions of relative friction at the bottom and top walls over the middle cross sections of the narrow channel and the dimple. Over the dimple middle cross section (Fig. 5a and b) at the bottom wall of the channel there is a group of dimples found in the earlier works: conical and spherical dimples and also an oval dimple of moderate lengthening. This group is characteristic of the developed separated flow forming in the dimple with the zone of substantial negative relative friction values. Here, it should be noted that the length of the separated flow zone is large for the conical dimple in comparison to the spherical one.

On the edge of the first-group dimples on the windward side, flow is sharply accelerated; maximum relative friction values appear to be close and high (of the order of 5–6). As the oval dimple length is increased, the maximum relative friction value on the dimple edge on the windward side monotonically decreases and at $b = 0.346$ (the cylindrical insert length is equal to 2) it practically drops and the ratio f/f_{pl} appears to be close to 1. The behavior of the dependence f/f_{pl} (x) for the oval dimples with the cylindrical insert length L of more than 1 is radically different from that of the similar dependences for the first-group dimples. Only in the vicinity of the dimple on the windward side the negative friction zone of small length is formed; maximum relative friction values in this zone are less than those for the first-group dimples. The oval dimple with $L = 1$ is also characterized by the formation of the negative friction zone of small length on the leeward side. In the center of oval dimples, friction is positive, i.e., the flow separation in the vicinity of the center of oval-trench dimples is not observed. The

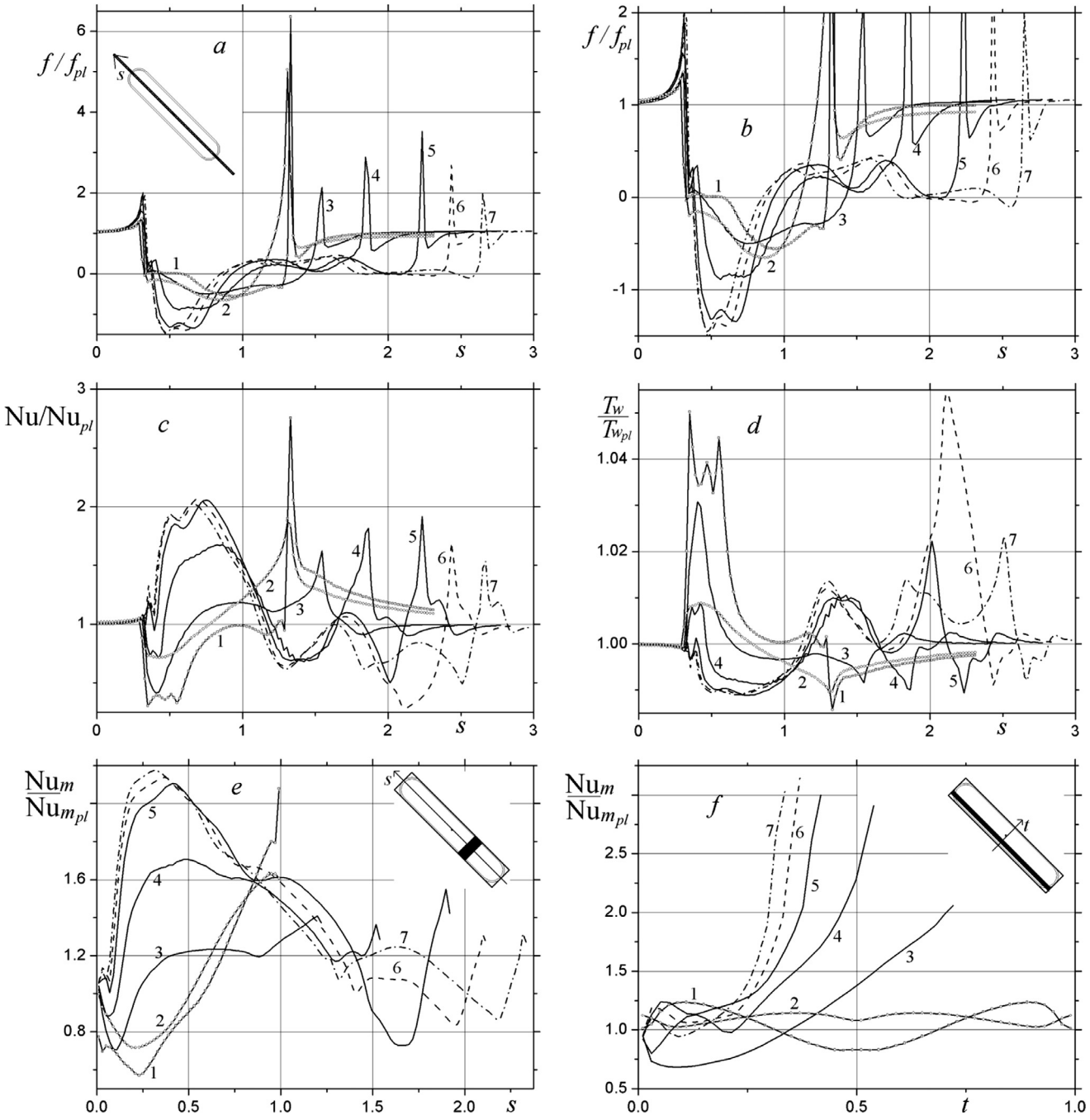

Fig. 6. Comparison of the dependences of relative friction (a,b), Nusselt number (c), wall temperature(d) averaged over transverse (e) and longitudinal (f) strips of the section surrounding the dimple, over middle longitudinal (a–e) and transverse (f) cross sections for single conical (1), spherical (2) and oval (3–7) dimples of different width: 3 – b = 0.731; 4 – 0.549; 5 – 0.429; 6 – 0.383; 7 – 0.346. b – fragment of the dependences in enlarged scale.

character of the dependence f/f_{pl} (x) for dimples with $L = 1$ and 1.5 is slightly different from that of the dependence for dimples with $L = 1.75$ and 2. The two-mode dependence is replaced by the one-mode dependence and is shifted along the coordinate to the edge of the dimple on the leeward side.

Flow in front of the first-group dimples is noticeably accelerated. Such flow acceleration for oval-trench dimples is not seen; in the dimple itself the ratio f/f_{pl} does not exceed 1, although at $L = 1.75$ and 2 the maximum relative friction value appears to be close to 1.

It is of importance to emphasize the relative friction behavior in the dimple wake. As mentioned, in the case of the first-group dimples, flow in the edge region is sharply accelerated (the maximum relative friction value substantially exceeds 1), but in the case of symmetric dimples (for the oval dimple with $L = 0.5$ the decrease is slightly less – up to 0.9), flow is fast decelerated and the ratio f/f_{pl} decreases within 0.5–0.7. For oval dimples with $L = 1$ and 1.5, the relative friction value also does not sharply decrease; after a maximum relative friction value has been attained on the windward side of the dimple, it monotonically decreases, remaining more than 1. For oval-trench dimples with $L = 1.75$ and 2, the behavior of the friction distribution slightly changes. First, flow in the dimple wake is decelerated and then undergoes slow acceleration. At that, the value of the ratio f/f_{pl} at a distance of 1 remains less than 1.

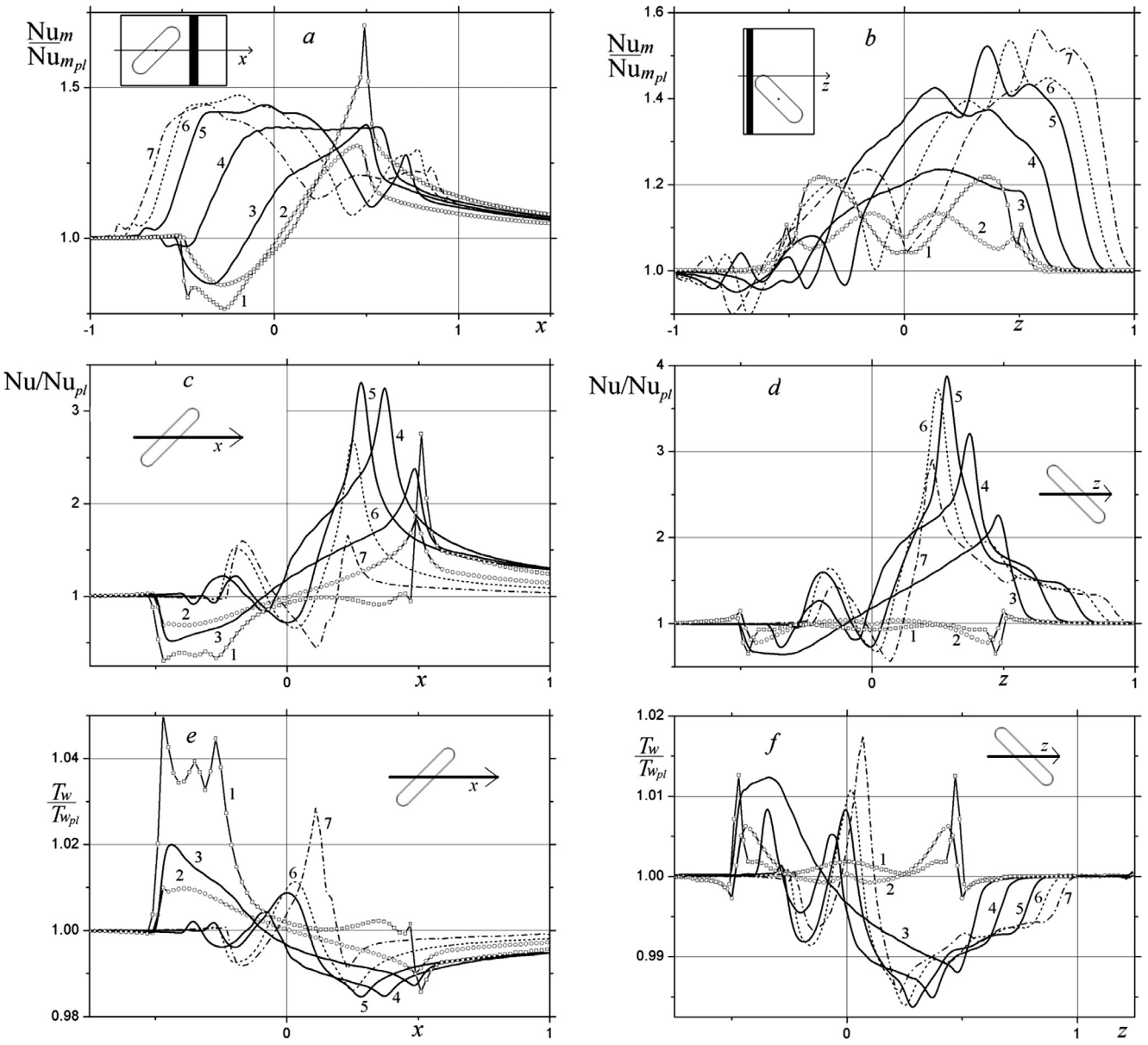

Fig. 7. Comparison of the dependences of relative local Nusselt numbers (c and d), and wall temperature (e and f) averaged over transverse (a) and longitudinal (b) strips of the dimpled section over middle longitudinal (a, c, and e) and transverse (b, d, and f) cross sections of the channel at the heated wall for single conical (1), spherical (2) and oval (3–7) dimples of different width: 3 – b = 0.731; 4 – 0.549; 5 – 0.429; 6 – 0.383; 7 – 0.346.

Over the channel middle cross section passing through the dimple center (Fig. 5c and d), the friction distribution behavior for symmetric dimples differs from that for oval ones. For symmetric dimples, maximum relative friction is practically absent on the side edges, whereas for oval dimples, such maximum friction is clearly defined, especially on the dimple edge on the windward side. As the oval dimple width is decreased, the maximum friction value increases, reaching 5 at $b = 0.549$ ($L = 1$). It should be noted that over the transverse cross section, it is higher than that over the longitudinal middle cross section for this dimple. As the dimple width is further decreased, the maximum friction value also decreases, but at $b = 0.346$ ($L = 2$), it exceeds by a factor of two the friction value at the plane-parallel channel wall (over the longitudinal middle cross section, the ratio f/f_{pl} is close to 1).

On the inner surface of symmetric dimples, the wall friction dependence is symmetric in character. The developed separated flow zone practically covers the inner surface of dimples over the transverse cross section. The maximum relative friction value decreases to 0.6. For the oval dimple of moderate lengthening ($L = 0.5$), the friction distribution is asymmetric in the transverse z-coordinate and the friction value changes sign on the windward side of the dimple; however, the separated flow zone occupies the inner surface of the dimple, and the backflow velocity is approximately the same as in the case of the conical dimple.

Flow and friction distributions undergo radical changes on the inner surface of oval-trench dimples (curves 4–7). As the dimple width is decreased over the transverse middle cross section, the changes in the plots are of the same type as those over the longitudinal middle cross section. However, if the two-mode behavior of the ratio f/f_{pl} is kept at $L = 1$, then at $L = 1.5$, it also looks like the single-mode one at $L = 1.75$ and 2. The maximum local relative friction value at $L = 1.5$ and 1.75 is close to 1, and at $L = 2$ it is approx. 0.8. In the narrow zone, on the oval-trench dimple edge on the windward side, the friction value is negative; at $L = 1.5$

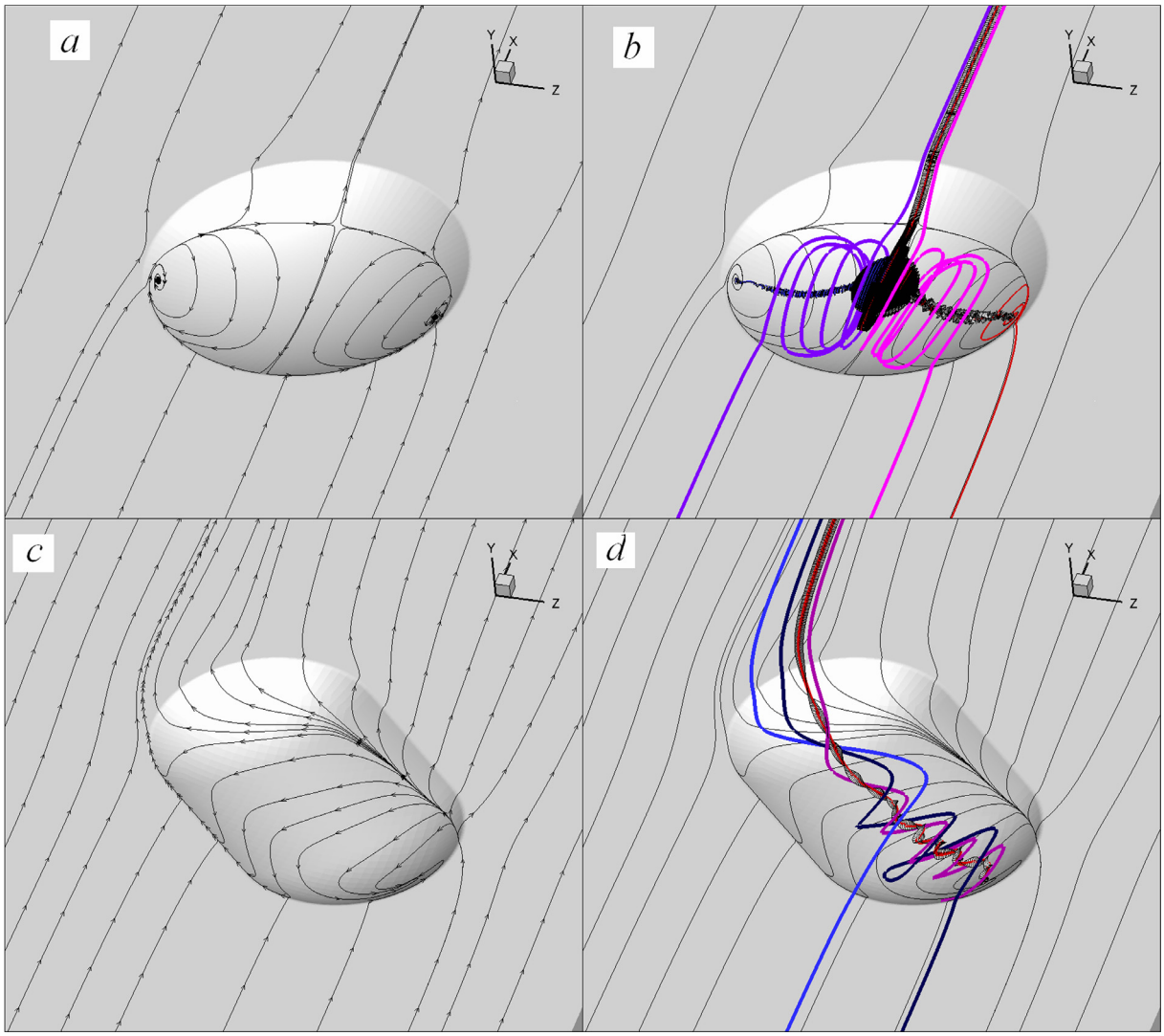

Fig. 8. Comparison of streamlines (a and c) and vortex structures (b and d) for spherical and oval (of width b = 0.731) dimples.

and 1.75, the minimum value of the ratio f/f_{pl} is comparable to the same value for the symmetric dimple.

For the oval dimple wake, the dependences f/f_{pl} (z) are very interesting. Starting with $L = 1$, from the right of the dimple edge there is a region of almost constant value in the distribution of relative friction of the order of 1.3–1.5; at that, behind it the relative friction value fast decreases to 1. The length of this region increases as the width of the dimple is decreased and its lengthening is increased (at $L = 2$ it reaches approx. 0.8). Undoubtedly, the presence of such a region of increased friction in comparison to the friction region at the plane-parallel channel wall gives an impetus to heat transfer enhancement in this region. It should be emphasized that such regions are not observed for symmetric dimples.

The pressure growth at the top plane wall of the channel above the first-group dimples (Fig. 4c) is accompanied by deceleration and subsequent acceleration of flow in this zone (Fig. 5e); at that, the maximum friction value is seen downstream from the dimple center by 0.5, whereas the minimum friction value is in the dimple center. As the oval dimple width is decreased (b is ranged from 0.731 to 0.429), the minimum and maximum local relative friction values reach 1, i. e., the dimple influence on flow near the top wall fast decreases. The minimum relative friction value in this case is observed upstream to the dimple center. However, the behavior of the dependences $f_{top}/f_{pl}(x)$ is the same. A transition to the oval-trench dimples of length $L = 1.75$ and 2 is reflected in the variation of the dependences; at that, the maximum relative friction value is shifted upstream to the dimple center and continues decreasing in magnitude.

The symmetric relative friction distribution along the transverse coordinate for symmetric dimples (Fig. 5f) corresponds to the static pressure distributions (Fig.4d); in what follows, the spherical dimple influence on flow deceleration at the top wall is more substantial (the ratio $f_{top}/f_{pl} = 0.8$) in comparison to the conical dimple (0.86). For the oval dimple of moderate lengthening ($L = 0.5$), the relative friction distribution becomes asymmetric, but the extent of the influence on flow deceleration near the wall is approximately the same as in the case of the 10°-truncated conical dimple (0.78).

As the oval dimple width is decreased and its length is increased, the minimum relative friction value increases, reaching 0.97 at $L = 2$. However, of most interest is the formation and growth of the maximum local relative friction value in the dimple center, staring with $L = 1$. At $L = 1.5$, it becomes practically equal to 1 and then increases to 1.07 at L = 1.75 and slightly decreases to 1.06 at $L = 2$. At that, the last maximum friction value is attained in the channel middle and corresponds to the oval-trench dimple

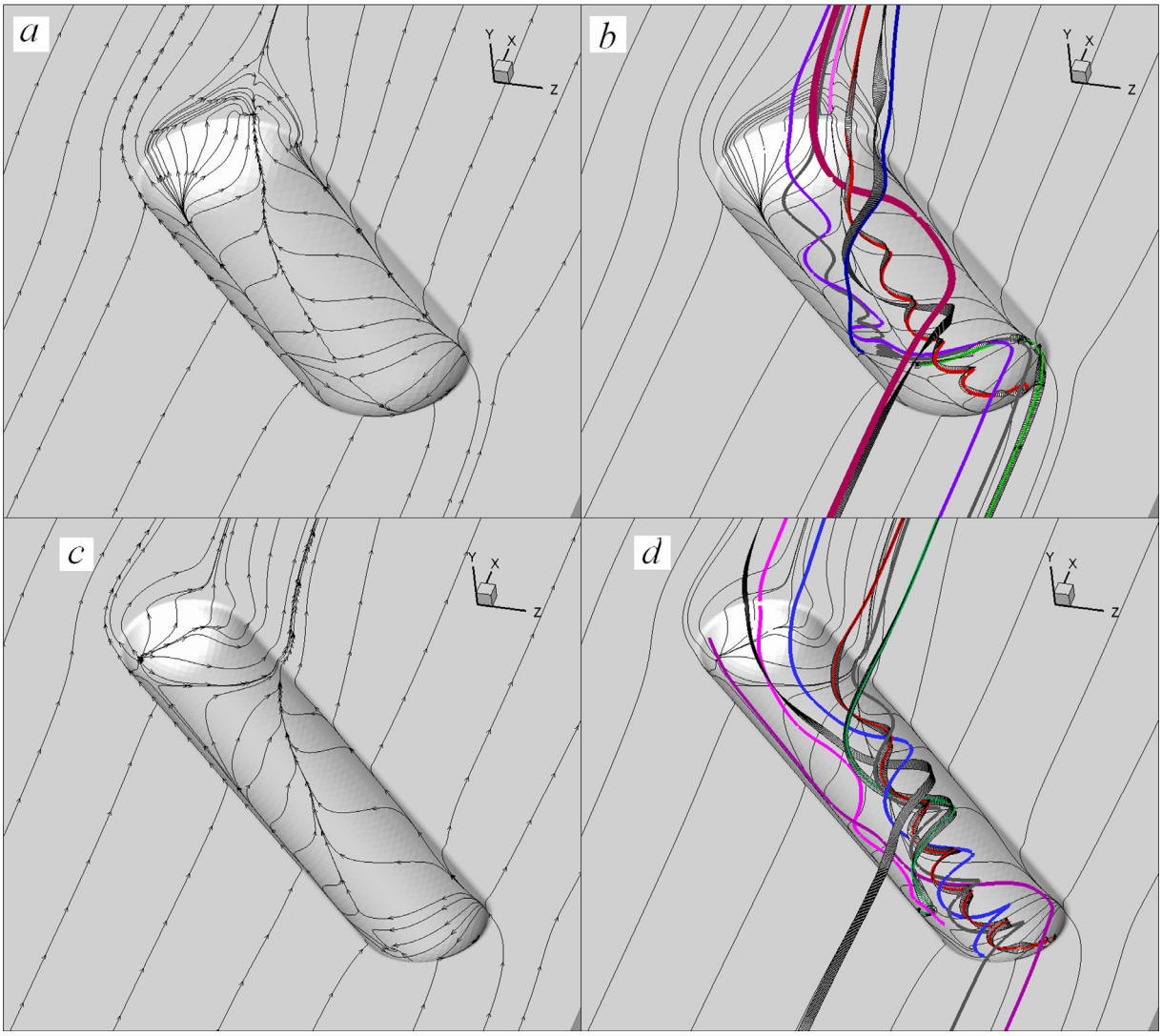

Fig. 9. Comparison of streamlines (a and c) and vortex structures (b and d) for oval dimples of width b = 0.549 and 0.429.

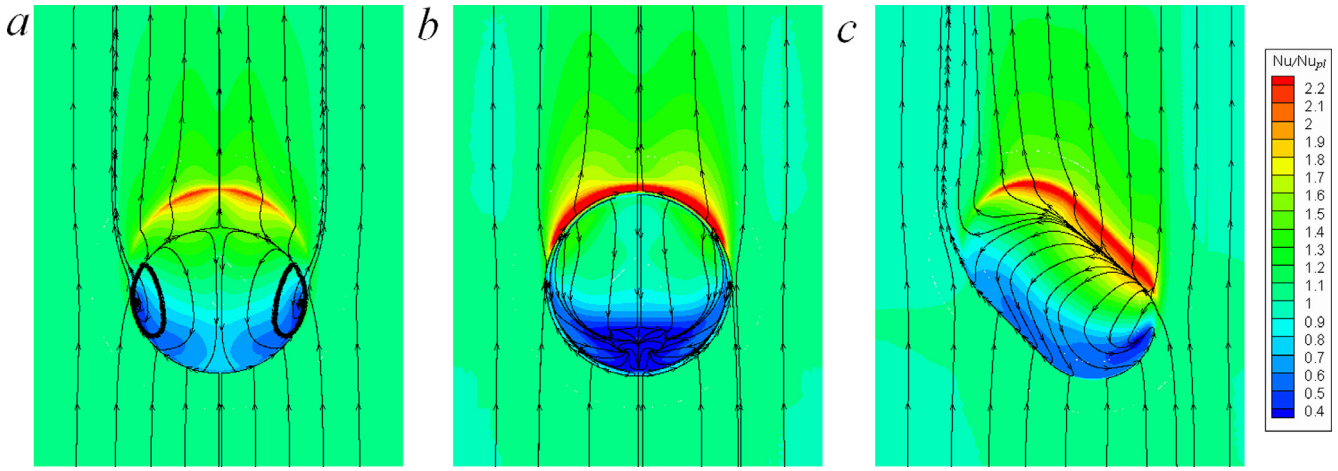

Fig. 10. Comparison of the variations of the relative Nusselt numbers at the heated wall with spherical (a) and conical (b) dimples, and also oval dimple (b = 0.731) with the streamlines.

center. The relative friction distribution for an actually oval-trench dimple with the lengthening of 6.78 (in terms of width) at a depth of 0.13 (approx. 39% of the channel height) with a maximum friction value along the coordinate to the channel center is indicative of the fact that flow in the narrow channel with the dimple at the bottom wall becomes in character peculiar to jet flow.

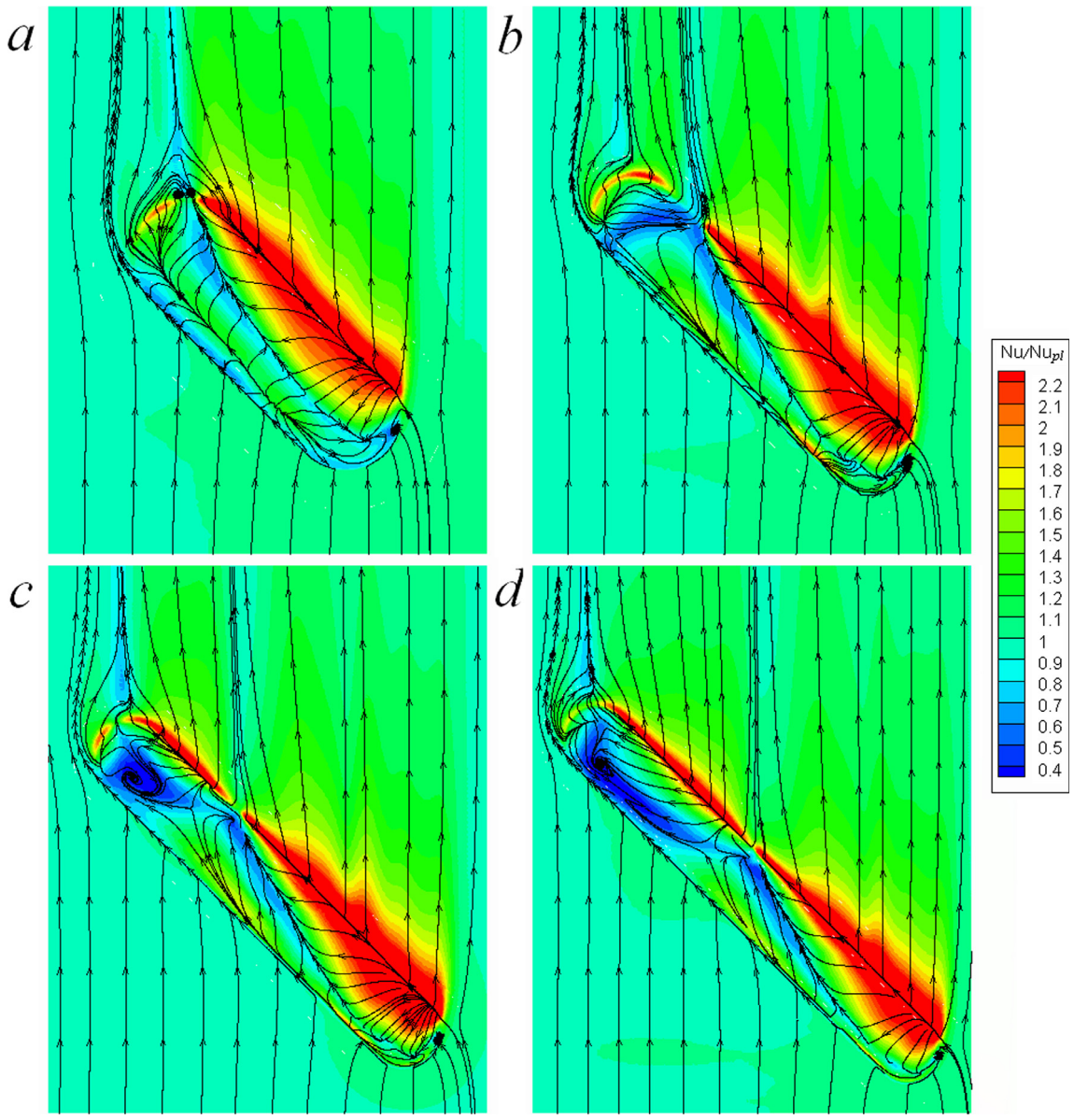

Fig. 11. Comparison of the variations of the relative Nusselt numbers at the heated wall with oval dimples of width b = 0.549 (a), 0.429 (b), 0.383 (c), 0.346 (d) with the streamlines.

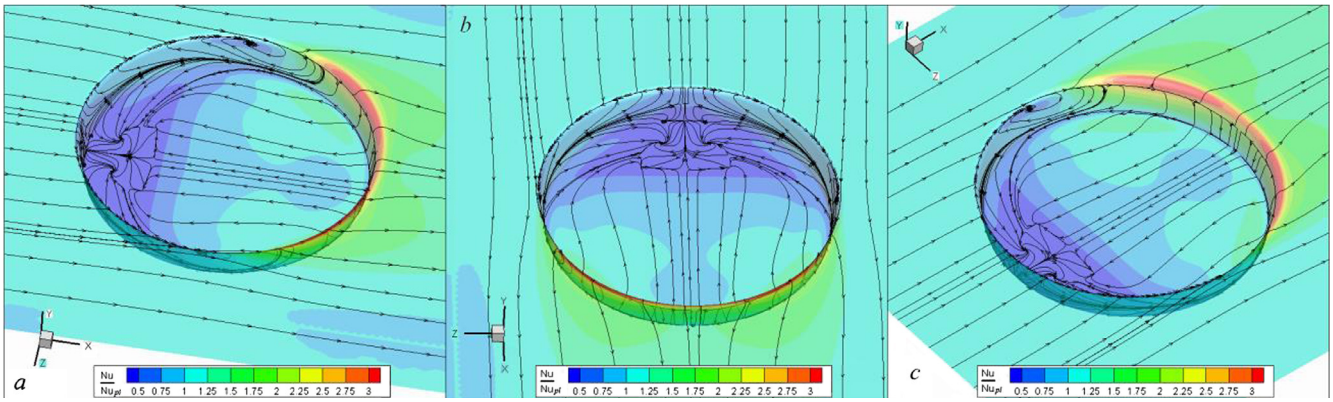

Fig. 12. Relative Nusselt number variations in the vicinity of the conical dimple prepared in three views.

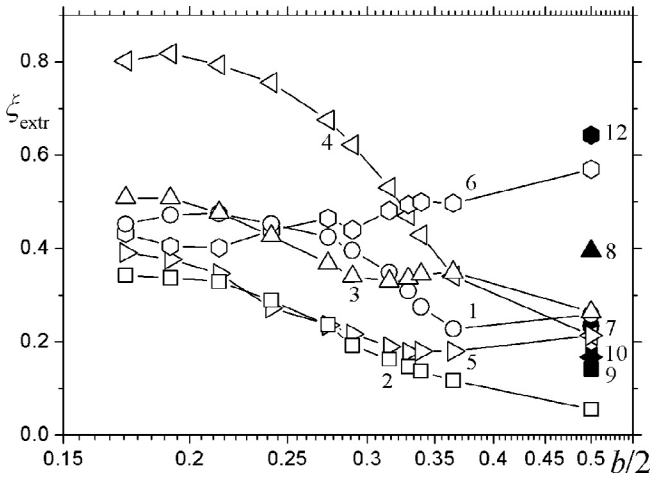

Fig. 13. Influence of the width b on the extremal characteristics of flow ξ extr. 1, 7 – (umin); 2, 8 – (−vmin); 3, 9 – vmax; 4, 10 – (−wmin); 5, 11 – wmax; 6, 12 – 10 kmax. 7–12 – conical dimple.

It is of significance to analyze the influence of the width of the oval dimple on the relative friction dependence $f/f_{pl}(s)$ over its central cross section where the s-coordinate is taken from the leading edge of the dimple (Fig. 6a and b). For comparison, this plot also presents the relative friction distribution over the middle cross section of the channel with spherical and conical dimples (Fig. 5a and b). The curves in Fig. 6a and b illustrate the observed change of the separated flow in the first-group dimples into the vortex flow when the separated flow zone is most clearly seen in the vicinity of the leading edge.

The first-group dimples including the oval dimples of moderate lengthening are characterized by the formation of a scale separated flow zone that covers almost the entire inner surface of dimples. As already mentioned, the minimum relative friction value is equal to −0.6 and a sharp increase in friction is seen on the trailing edge of dimples. However, the maximum friction value for the oval dimple of width $b = 0.731$ is not high and is equal to 2.

When the length of the oval dimple is increased and its depth is maintained, the narrowing of this dimple results both in a gradual localization of the separated flow zone and in the backflow augmentation in it. Moreover, the separated flow zone is followed by the flow acceleration region with a maximum local relative friction value of the order of 0.3–0.4. The oval dimple with $L = 1$ can be considered intermediate since the values of the separated flow zone length and minimum relative friction in it are still far from the steady-state values. Starting with $L = 1.5$, the separated flow zone and the minimum relative friction value in the oval dimple are stabilized and rather slightly depend on its width and length, although, as seen from Fig. 6b, when the oval dimple width is decreased, the separation point is slightly shifted to the leading edge. It can be stated that the separated zone length in terms of dimple width is constant for oval-trench dimples. The separated flow rate in oval-trench dimples appears to be noticeably higher than in the first-group dimples. The minimum relative friction value is of the order of −1.5.

In the middle of the oval-trench dimple with $L = 1.5$–2, it is possible to select the flow acceleration zone; at that, the relative friction dependences $f/f_{pl}(s)$ are close. Further, the decelerated flow zone is formed in oval-trench dimples with $L = 1.75$–2. In the vicinity of the trailing edge, the maximum relative friction value increases, monotonically reaching 3.5 as L is ranged from 0.5 to 1.5 and then it gradually decreases up to 2 at $L = 2$.

Behind the trailing edge, the decelerated flow zone with the minimum relative friction value (0.7–0.8) is observed and comes to an end when the friction attains the friction level at the plane-parallel channel wall.

Unlike the earlier considered curves in Fig. 5, the flow region near the leading edge of the oval dimple (Fig. 6) is characterized by flow acceleration and two-fold increased relative friction.

4.3. Local and integral Nusselt number distribution. temperature fields

Figs. 6c–f and 7 demonstrate the linear distributions of the relative temperature, the local relative Nusselt number and the strip-averaged Nusselt number, as well as the temperature and the relative Nusselt number on the streamlined surfaces over the middle cross sections of the narrow channel and dimples, and also the streamlines. The investigation methodology was developed on the basis elsewhere described in [38,40] and extended to oval dimples, whose contour was assumed to be surrounded with a rectangular control region and to be treated in the manner done in the analysis of the characteristics of the rectangular region around the spherical dimple. Fig. 6c and d plots the ratios Nu/Nu_{pl} and T_w/T_{wpl} over the longitudinal middle cross section of the channel with spherical and 10°-truncated conical dimples.

The distribution of the relative local Nusselt number over the middle cross section of the oval dimple in Fig. 6c shows that for symmetric and oval dimples with the cylindrical insert of length $L = 0.5$, the length of the zone of decreased relative heat loads is large enough; at that, for the conical dimple the ratio Nu/Nu_{pl} decreases up to 0.3 and does not exceed 1 practically within the entire dimple space. In the case of spherical and oval dimples, relative heat transfer increases only on the edge of the dimples on the windward side. It should be noted that in the symmetric dimple wake, there occurs the zone of moderate heat loads, exceeding those at the heated wall of the plane-parallel channel. Behind oval dimples such long zones are not seen and the ratio Nu/Nu_{pl} very fast becomes equal to 1.

As the oval dimple width is decreased, the relative Nusselt number distribution changes. Similarly to the maximum relative friction growth (Fig. 6a), the maximum value of Nu/Nu_{pl} increases in the vicinity of the trailing edge of the oval dimple with L ranging from 0.5 to 1.5 and then decreases from 1.9 to 1.5 (at $L = 2$). It is surprisingly interesting to see a substantial increase of the relative Nusselt number in the separated flow zone (the relative friction value is less than zero). In the region of the leading edge on the leeward side, the maximum value of Nu/Nu_{pl} reaches 2; it is being known that the region of the increased Nusselt numbers much (approximately two times) exceeds the length of the separated flow zone. As in the case of the relative friction distributions, the distributions $Nu/Nu_{pl}(x)$ at $L = 1.5$–2 are rather close.

In oval-trench dimples, the enhanced heat transfer area adjacent to the leading edge is followed by a small region where the value of Nu/Nu_{pl} is low (less than 1) and then the narrow region of low elevated heat loads is again followed by a very long region where the value of Nu/Nu_{pl} is low; it extends to the trailing edge of the oval dimple. It should be noted that at $L = 1.75$, the minimum value of Nu/Nu_{pl} in the vicinity of the trailing edge is approx. 0.3.

In many ways, such a behavior of the Nusselt number is defined through the wall temperature (Fig. 6d). So, the marked minimum value of heat loads corresponds to the maximum value of T_w/T_{wpl} equal to 1.055. Attention is drawn to the fact that high wall temperatures in the conical dimple and in the oval dimple of moderate lengthening correlate with the low level of heat transfer in separated flow zones. At the same time, the supercooling of the surface of the dimple, i.e., a decrease in its temperature below the level characteristic of the plane-parallel channel wall, is accompanied by the heat transfer growth; for example, it is seen in the vicinity of the region of the trailing edge on the windward side and in the near-wake region.

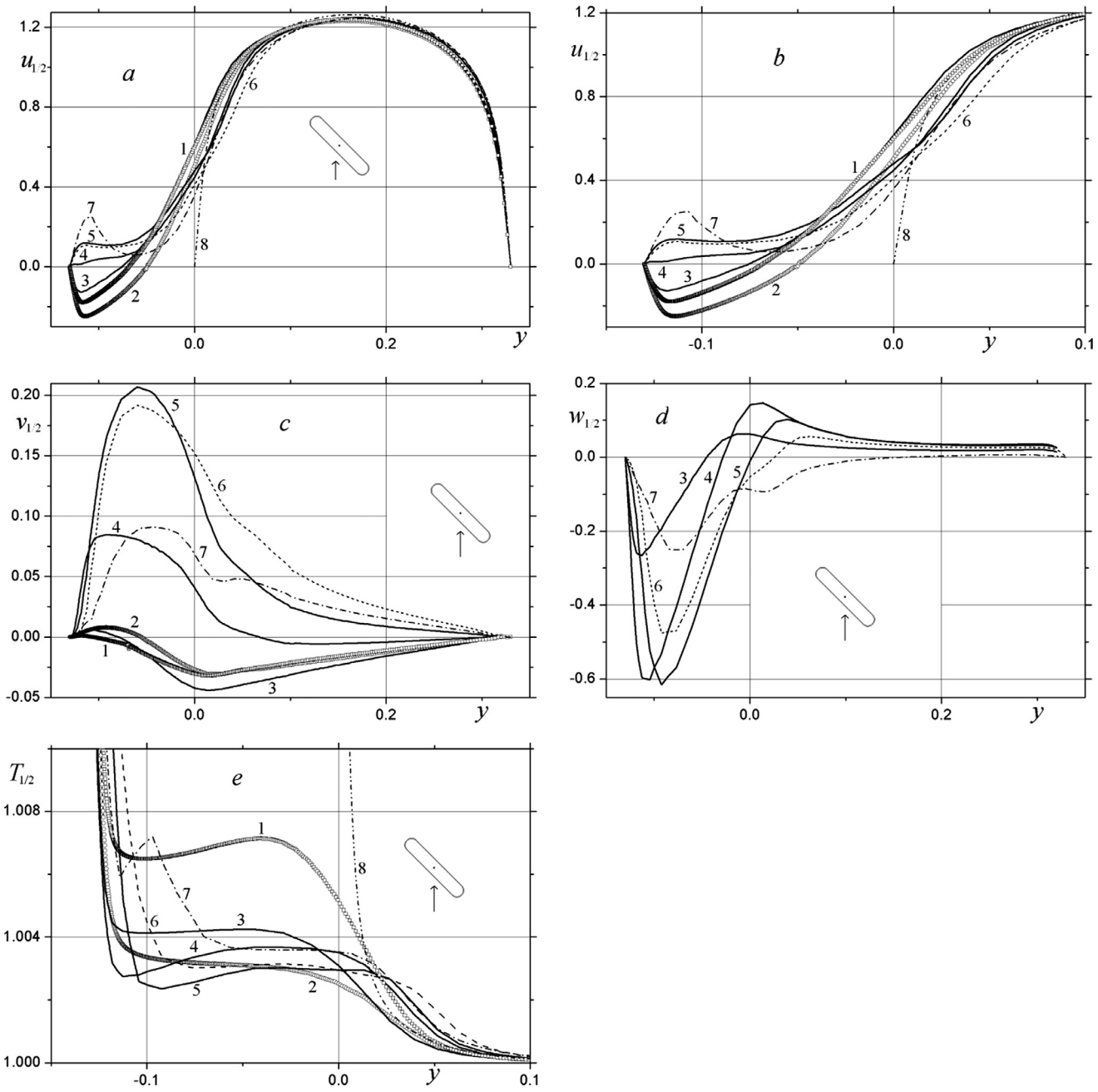

Fig. 14. Comparison of the profiles of longitudinal (a and b), vertical (c) and transverse (d) velocity components, temperature (e) in the centers of single conical (1), spherical (2) and oval (3–7) dimples of different width: 3 – b = 0.731; 4 – 0.549; 5 – 0.429; 6 – 0.383; 7 – 0.346.; 8 – plane-parallel channel; b – fragment of the dependences in enlarged scale.

As the oval dimple cylindrical insert of length L is more than 1, the value of the ratio T_w/T_{wpl} for the separated flow zone becomes less than 1. The region of dimple supercooling coincides with that of enhanced heat transfer, whereas the regions of increased temperatures, vice versa, correspond to those of low heat transfer.

As mentioned in [38,40], the relative Nusselt number (Nu_m/Nu_{mpl}) averaged over the transverse (Fig. 6e) and longitudinal (Fig. 6f) strips of the region surrounding the oval dimple gives an idea of the physical mechanism of thermal efficiency of a surface vortex generator.

For the symmetric dimples and the oval dimple of width $b = 0.731$, the low heat transfer regions are largely compensated by the high heat transfer ones; however, the thermal efficiency is low.

As the width of the oval dimple is decreased and its length is increased, the dependences $Nu_m/Nu_{mpl}(x)$ demonstrate the increase in heat transfer practically within the entire region of the dimple, starting with $L = 1.5$, the ratios Nu_m/Nu_{mpl} appear to be close to those within the region of the length of about 1.4. The maximum value of Nu_m/Nu_{mpl} reaches 1.9. About the half of the oval-trench dimple is effective when increasing heat transfer. The long region adjacent to the trailing edge is characterized by a relatively low value of Nu_m/Nu_{mpl}, but exceeding 1. It should be noted that there exist the narrow regions with a low value of Nu_m/Nu_{mpl}.

The variations of Nu_m/Nu_{mpl} in the transverse t-coordinate demonstrate the extreme heat transfer nonuniformity across the oval dimple. On the windward side of dimples, relative heat trans-

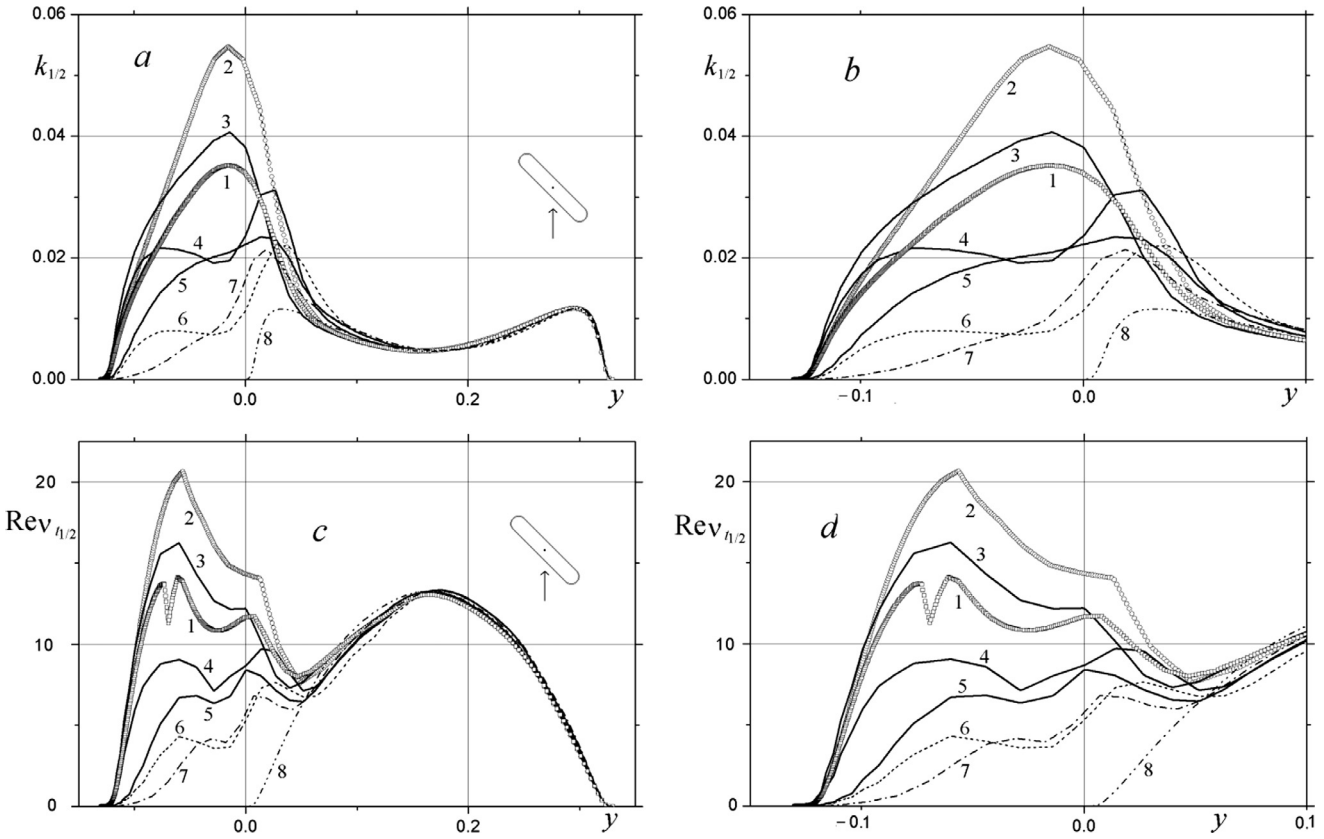

Fig. 15. Comparison of the profiles of turbulence energy (a and b) and normalized vortex viscosity (c and d) in the centers of single conical (1), spherical (2) and oval (37) dimples of different width: 3 – b = 0.731; 4 – 0.549; 5 – 0.429; 6 – 0.383; 7 – 0.346; 8 – plane-parallel channel; b and d – enlarged fragments in the vicinity of the dimple.

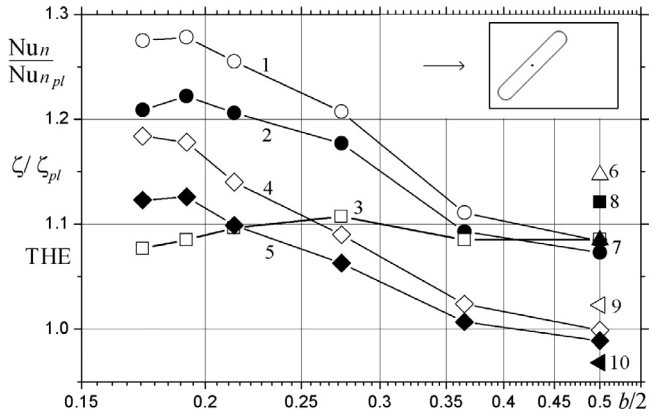

Fig. 16. Influence of the oval dimple width b on thermal (1, 2, 6, and 7) and thermalhydraulic (4, 5, 9, and 10) efficiencies, as well as relative hydraulic losses (3 and 8); 6–10 – conical dimple; 2, 5, 7, and 10 – with regard to the area of the dimple inner surface over the 3 × 2 section and the shift of the dimple center by 1 from the front boundary.

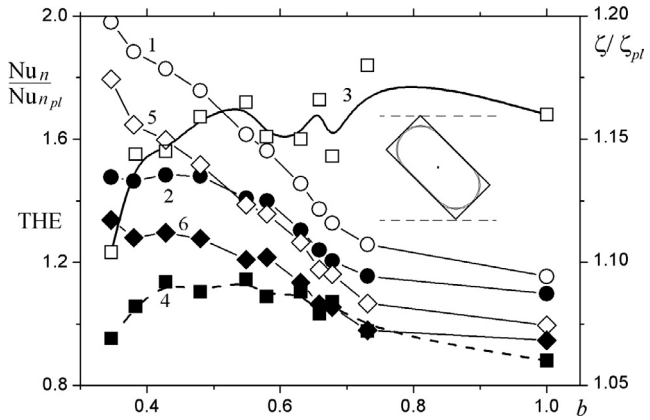

Fig. 17. Influence of the oval dimple width b on thermal (1 and 2) and thermal hydraulic (5 and 6) efficiencies, as well as relative hydraulic losses (3 and 4); 2,6 – with regard to the area of the dimple inner surface; dashed curve (4) – Table 3 data.

fer grows three times. However, on the leeward side, its level is very insignificant. About the third of the dimple width does not participate in the process of heat transfer enhancement. Nevertheless, oval-trench dimples of large lengthening are more preferable in thermal efficiency in comparison to the first-group dimples.

Fig. 7 analyzes the distributions of thermal characteristics over the longitudinal and transverse middle cross sections of the channel at different shapes of dimples and at different widths of the oval dimple.

The dependences of the relative Nusselt number averaged over the transverse and longitudinal strips are built for the 2.5 × 2 rectangular section when the dimple center is located at a distance of 1 from the front boundary (Fig. 7a and b). Of the dimples considered, the conical dimple (curve 1) is characterized by the largest maximum value among the maximum values of Nu_m/Nu_{mpl} over the longitudinal middle cross section of the channel: it is equal to 1.7 and its position corresponds to the trailing edge of the dimple on the windward side. As previously mentioned, heat transfer from the conical dimple bottom is extremely low and total heat removal is provided by the side walls in the windward region. For the spherical dimple, very moderate (of the order of 1.3) maximum relative heat transfer occurs due to the position of the dimple on the windward side. The oval dimple of width $b = 0.731$ insignificantly differs

Table 2
The comparison of the refined extremal characteristics of flow and heat transfer in the narrow channel with single spherical, conical and oval dimples of variable width at constant depth and spot area.

b	χ	u_{min}	v_{min}	v_{max}	w_{min}	w_{max}	k_{max}	v_{tmax}	T_{wmax}
Cone	1	−0.234	−0.141	0.395	−0.167	0.167	0.0643	0.00231	1.104
1	1	−0.258	−0.055	0.264	−0.214	0.214	0.0570	0.00234	1.054
0.731	1.68	−0.228	−0.117	0.349	−0.341	0.180	0.0497	0.00194	1.062
0.678	1.92	−0.275	−0.137	0.345	−0.429	0.180	0.0500	0.00207	1.053
0.659	2.02	−0.309	−0.147	0.336	−0.470	0.178	0.0494	0.00206	1.053
0.631	2.19	−0.349	−0.163	0.330	−0.531	0.190	0.0481	0.00202	1.053
0.58	2.55	−0.396	−0.192	0.340	−0.622	0.217	0.0440	0.00187	1.053
0.549	2.82	−0.424	−0.236	0.368	−0.676	0.236	0.0465	0.00185	1.053
0.482	3.59	−0.453	−0.289	0.427	−0.756	0.273	0.0439	0.00162	1.053
0.429	4.50	−0.475	−0.329	0.477	−0.794	0.346	0.0402	0.00147	1.053
0.383	5.57	−0.472	−0.337	0.508	−0.818	0.377	0.0405	0.00142	1.085
0.346	6.78	−0.452	−0.343	0.509	−0.802	0.391	0.0432	0.00141	1.086

Table 3
The comparison of thermal and thermal-hydraulic characteristics of two sections of the narrow channel with single spherical, conical and oval dimples of variable width at constant depth and spot area.

b	Nu_{n1}/Nu_{npl1}	ζ_1/ζ_{pl1}	$(Nu_{n1}/Nu_{npl1})/(\zeta_1/\zeta_{pl1})$	Nu_{n2}/Nu_{npl2}	ζ_2/ζ_{pl2}	$(Nu_{n2}/Nu_{npl2})/(\zeta_2/\zeta_{pl2})$
Cone	1.147 (1.085)	1.121	1.023 (0.968)	1.378 (1.076)	1.289	1.069 (0.835)
1	1.063 (1.054)	1.061	1.002 (0.993)	1.138 (1.083)	1.16	0.981 (0.934)
0.731	1.099 (1.084)	1.072	1.025 (1.011)	1.258 (1.155)	1.18	1.066 (0.979)
0.678	1.112 (1.096)	1.084	1.026 (1.011)	1.327 (1.205)	1.145	1.158 (1.051)
0.659	1.122 (1.105)	1.079	1.040 (1.024)	1.372 (1.240)	1.166	1.177 (1.063)
0.631	1.137 (1.118)	1.088	1.045 (.028)	1.455 (1.304)	1.15	1.265 (1.134)
0.58	1.159 (1.138)	1.086	1.067 (1.048)	1.562 (1.400)	1.151	1.357 (1.216)
0.549	1.172 (1.149)	1.093	1.072 (1.051)	1.616 (1.408)	1.165	1.387 (1.209)
0.482	1.197 (1.167)	1.088	1.100 (1.073)	1.758 (1.48)	1.159	1.517 (1.277)
0.429	1.209 (1.172)	1.092	1.107 (1.073)	1.829 (1.484)	1.145	1.597 (1.296)
0.383	1.222 (1.177)	1.082	1.129 (1.088)	1.884 (1.464)	1.144	1.647 (1.280)
0.346	1.243 (1.190)	1.069	1.163 (1.113)	1.981 (1.477)	1.104	1.794 (1.338)

from the spherical one. The mentioned group of dimples is characterized by the low values of the relative averaged Nusselt number because of the developed separated flow formation and the high temperature value on the leeward side of the dimple. It is interesting to note that in the wake behind this-group dimples, heat transfer decreases, remaining slightly higher than heat transfer at the plane-parallel channel wall.

As the width of the oval dimple is decreased and its length is increased, the dependence $Nu_m/Nu_{mpl}(x)$ undergoes changing. First of all, total heat load is leveled in the vicinity of the dimple and the value of Nu_m/Nu_{mpl} becomes constant. The maximum value of the relative averaged Nusselt number reaches 1.45 at $L = 1.75$. The curves for Nu_m/Nu_{mpl} at L = 1.5, 1.75, 2 are gradually shifted upstream; it is true that a sharper decrease in heat transfer is seen for the last oval-trench dimple. Moreover, at L = 1.75 and 2, the minimum and maximum local values of Nu_m/Nu_{mpl} appear.

Fig. 7b shows the re-construction of the symmetric dependences of Nu_m/Nu_{mpl} for the conical (curve 1) and spherical (curve 2) dimples into the asymmetric dependences for oval dimples (curves 3–7). Curve 3 for the dimple of width 0.731 covers the curves with two symmetric maximum values for symmetric dimples; however, there is the strip-averaged longitudinal low relative Nusselt number region that passes through the vicinity of the trailing edge of the dimple. The maximum value of the dependence $Nu_m/Nu_{mpl}(z)$ exceeds the similar maximum value for the conical dimple and is seen to the right of the dimple center.

Subsequent curves 4–7 represent the dome-shaped dependences with increasing values shifting to the right of the center; the maximum value of Nu_m/Nu_{mpl} increases up to 1.55 for $L = 2$. With increasing the dimple length, on the left edge the maximum local value of Nu_m/Nu_{mp} appears, grows and is shifted to the right, leaving the narrow zones of low relative heat loads (for $L = 1.75$ and 2) near the left edge.

It is interesting to consider the relative local Nusselt number over the longitudinal and transverse middle cross sections of the channel (Fig. 7c and d) in combination with the relative friction dependences (Fig. 6a–d) that have already been analyzed. The revealed earlier selection of the group of symmetric dimples added

with the oval dimple of width $b = 0.731$ is justified in this case. Maximum relative heat loads in the vicinity of the trailing edge on the windward side are over the range 1.8–2.8; in the low heat transfer zone, the minimum values of Nu/Nu_{pl} vary from 0.3 to 0.7. The maximum relative friction value for these dimples ranges from 5 to 6.5 and is largest for all considered dimples. For oval dimples with $L = 1$ and 1.5, the maximum value of Nu/Nu_{pl} in the edge region appears to be noticeably higher than that for the first-group dimples and reaches 3.3. It is of interest to note that in this case, a maximum local value appears in the vicinity of the dimple edge on the leeward side. It should also be emphasized that the low relative Nusselt number regions exist in the center of oval dimples. In passing from $L = 1.75$ to 2, the maximum values decrease on the right edge and increase up to 1.5 on the left edge.

Over the transverse cross section of symmetric dimples the Nu/Nu_{pl} variations are very small in comparison to oval dimples. The maximum relative Nusselt number value grows from 2.2 to 3.8 with increasing L from 0.5 to 1.5, then it decreases to 2.8 for the oval-trench dimple with $L = 2$. In the vicinity of the left edge on the leeward side at $L = 1.5$–2, the maximum local value of heat load grows to 1.5, and at $L = 2$ in the dimple center there occurs the region of the low values of the relative Nusselt number with its minimum value equal to 0.5.

The values of the dependences $Nu/Nu_{pl}(z)$, described by curves 4–7, in the right part of the selected vicinity in the oval dimple wake slightly change up to the range of $z = 1.25$–1.5 and then sharply decrease. As the oval dimple width is decreased, the regions of the decreased values of these dependences are shifted to the right.

Fig. 7e and f compares the longitudinal and transverse distributions of the relative wall temperature over the middle cross section of the dimpled channel.

The relative temperature value at the conical dimple bottom near the leading edge increases up to 1.05, whereas for the spherical dimple the superheating value at this very place is much less and is equal to 1.01. For the oval dimple of width $b = 0.731$, it is twice as large (1.02). In the vicinity of the right edge on the windward side, the wall is supercooled, and the relative temperature value ranges from 0.986 to 0.99 for the dimples mentioned.

The increase in the oval dimple length from $L = 1$ to 2 radically changes the dependence $T_w/T_{wpl}(x)$. The low temperature zone (the minimum local value at $L = 2$ is equal to 0.992) is formed on the leeward side. In the dimple center, there appears a maximum local relative temperature value increasing from 1.003 at $L = 1$ to 1.03 at $L = 2$. In this case, on the windward side and in the dimple wake the ratio $T_w/T_{wpl} < 1$. A minimum local relative temperature value in this zone first decreases to 0.983 at $L = 1.5$ and then increases to 0.992 at $L = 2$.

In the transverse direction, the variation of the dependence $T_w/T_{wpl}(z)$ is slightly less than in the longitudinal direction. The maximum relative temperature value on the side edge of the conical dimple does not exceed 1.012 and the supercooling value in front of the edge is 0.998. On the left edge of the oval dimple of width $b = 0.731$, the maximum relative superheating value is 1.012, whereas on the right edge it is 0.989, i. e., it is much larger than for symmetric dimples. The decrease in the oval depth width and the increase in its length while maintaining its depth changed the behavior of the dependence $T_w/T_{wpl}(z)$. At $L = 1$, two maximum local values and two minimum local values of the dependence appeared; the first maximum value and the last of the minimum values evolved from the maximum and minimum values of the dependence $T_w/T_{wpl}(z)$ at $L = 0.5$. It is interesting to note that the first maximum value vanished with a further growth of L. As the dimple width was decreased, the first minimum local value decreased to 0.992 at $L = 1.5$, and then slightly increased to 0.993. The maximum value in the dimple center monotonically increased from 1.005 to 1.017 and was shifted to the right (L increased from 1 to 2). The second minimum local value decreased to 0.983 at $L = 1.5$ and then increased to 0.986 at $L = 2$, gradually shifting to the left.

In the zone behind the dimple, on the right side the low relative temperature zone is expanding. As relative local heat transfer, the temperature also slowly ranges within 0.992–0.995 and then sharply decreases.

The computer visualization of 3D vortex structures in oval dimples is made with the use of the method of labeled particles, as done in [38,40]. Particles are injected in the vicinity of source- and sink-type singularities that are defined through the streamlines over a dimpled curvilinear surface. The trajectories of liquid particles are calculated with the use of the Cartesian velocity components determined from the solution of the fluid dynamics problem.

As known, in the case of flow around the moderate-depth spherical dimple, at the narrow channel wall, the symmetric pair of vortices is formed in the separated flow zone (Fig. 8). On the side edges of the dimple, the focus-type singularities (Fig.8a) are located, in the vicinity of which the vortex flows interacting in the symmetry plane are generated. As shown in Fig. 8b, the streamlines enter the dimple from the incoming flow. As a result, a radial jet issuing in the vicinity of the symmetry plane is formed.

In the case of flow around the oval dimple of width $b = 0.731$, in the vicinity of the leading edge of the dimple the streamlines (Fig. 8c) also have a focus-type singularity, in the vicinity of which the vortex is generated. In Fig. 8d it is shown how it is formed from the particles entering the dimple from the incoming flow. The vortex flow is issuing in the vicinity of the trailing edge of the dimple. Near the wall, the flow inside the dimple is reciprocal-circulation in character.

From the streamlines over the surface of the oval dimple with the cylindrical insert of length $L = 1$, it is seen that the larger part of the inner surface of the dimple is streamlined without flow separation (Fig.9a). Fig. 9b shows the trajectories of the labeled particles that have been injected in the vicinity of the focus-type singularity on the leading edge and have entered the dimple from the external flow. They demonstrate several configurations of vortex structures consistent with the streamlines at the wall inside the dimple. So, it is interesting to consider a small-diameter spiral vortex adjacent to the edge of the dimple on the windward side. As a whole, the system of vortices is issuing in the vicinity of the trailing edge.

For the dimple with the cylindrical insert of length $L = 1.5$, the main feature of the streamlines (Fig. 9c) is the vortex flow issuing through the part of the oval dimple on the windward side, not reaching the trailing edge of the dimple. The location of the issuing flow is associated with the concentration of streamlines on the dimple surface. The visualization of spiral structures showed (Fig. 9d) that the trajectories of labeled particles are concentrated in large quantities in this zone.

The variations of temperature fields and streamlines with decreasing oval dimple width should be added together with the comparison of relative Nusselt numbers fields. For oval and conical dimples, Figs. 10–12 show these variations in different scale and in different color and the streamlines.

According to the classification, the dimples of the first group combining symmetric dimples and oval dimples of width $b = 0.731$ cannot be considered effective from the viewpoint of increase in heat transfer from the dimpled heated wall of the narrow channel. As seen from Fig. 10, the increased relative Nusselt number regions are rather narrow and short. In addition, the low heat transfer areas are peculiar to such dimples. They are especially long for 10°-truncated conical dimples (Fig. 12). However, it is of importance to note that heat transfer is enhanced in them on the side edges of the dimple, although, as will be shown, hydraulic losses in channels with such dimples are very high.

The oval-trench dimples with the cylindrical insert of lengths $L = 1, 1.5, 1.75, 2$ (Fig. 11) are undoubtedly more promising; in this figure the red color shows the regions located not only in the dimple wake, but also inside the dimple. Although in the vicinity of the trailing edge, the low heat transfer areas exist, growing with increase in relative dimple lengthening, their development is to certain extent compensated by expanding the enhanced heat transfer area on the side edge of the dimple on the windward side in the vicinity of the trailing edge.

4.4. Velocity distributions

Figs. 13 and 14 and Table 2 present the results on the extreme local Cartesian velocity components and turbulence characteristics in the narrow channel with the 10°-truncated conical and oval dimples of different width at a depth of 0.13 and a fixed spot area.

The plots of the behavior of extreme turbulent flow characteristics in the channel and the data of Table 2 largely explain the advantage of oval-trench dimples. As the width b is decreased, secondary flow in the dimple first defined by the maximum and minimum values of the transverse velocity component (curves 4 and 5) is dramatically augmented; at that, other extreme velocity components also grow in absolute magnitude. Of course, it is necessary to take into account the increase in the relative dimple depth defined by the ratio of the fixed depth (0.13) to the constantly decreasing width and the ratio value reaching 0.39 at $L = 2$.

The reciprocal-circulation flow velocity estimated by the module of the minimum separated flow velocity u_m increases from 0.23 to 0.475 as the oval dimple length is increased from $L = 0.5$ to 1.5; at the stage of completing and localizing the separation zone at $L = 0.9$, the magnitude $|u_m| = 0.4$. When the length L is increased by a factor of more than 1.5, the value of $|u_m|$ slightly decreases to 0.45 at $L = 2$. It should be noted that in the spherical dimple, the value of $|u_m|$ appears to be much larger (0.26) than in the oval dimple of width $b = 0.731$ (0.23), whereas in the case of the conical dimple, practically there is no difference as compared to the considered oval dimple.

The behavior of ascending flows is often indicative of the restructuring of the separated flow. Here, it should be noted that there is a minimum local value of $v_{max} = 0.33$ between $L = 0.75$ and 0.9. Just over this range of the cylindrical insert length the separated flow zone is stabilized in the case of the oval dimple. It is interesting to emphasize that in going from the spherical dimple to the oval dimple of width $b = 0.731$, the value of v_{max} rather sharply increases from 0.26 to 0.35. As the oval dimple width is decreased, the increase in v_{max} is stabilized and reaches 0.51 at $L = 1.75$–2. The maximum value of the descending flow velocity $(-v_{min})$ gradually increases from 0.06 ($L = 0$) to 0.34 ($L = 2$); at that, there are no jumps in going to oval dimples. For the conical dimple, the values of $(-v_{min})$ and v_{max} appear to be much higher than those for the spherical dimple: 0.14 and 0.4, respectively.

One of the most important results of this work is the revealed effect of a sharp increase in $(-w_{min})$ for oval dimples with the cylindrical insert of length of more than 1.5. The negative minimum value of the secondary flow velocity increases almost four times (in comparison to the spherical dimple) and reaches 0.81 of the bulk velocity in the channel.

In what follows, the maximum transverse velocity component w_{max} slightly changes at the stage of restructuring the separated flow in the case of the oval dimple (from $L = 0.5$ to 0.9), remaining at a level of 0.18. Further, w_{max} monotonically grows to 0.39 at $L = 2$.

Of big interest are the maximum temperatures at the dimpled heated wall (Table 2). In fact, for all dimples, except the conical and oval dimples with the insert of lengths $L = 1.75$, 2, they are the same and are likely not realized in the dimples. In the conical dimple, the maximum value of T_w appears at its bottom in the vicinity of the leading edge of the dimple on the leeward side, whereas in the oval-trench dimple, a very long spot with a high temperature T_w is formed in the vicinity of the trailing edge.

In Fig. 14, the profiles of the Cartesian velocity components and the temperature in the dimple center reflect the evolution of flow and temperature field in the dimple as its width is decreased.

The first-group dimples are characterized by the formation of the separated flow with a negative component $u_{1/2}$. The maximum value of the backflow velocity for the conical dimple (0.25) exceeds the similar maximum values for the spherical dimple (0.2) and the oval dimple of width $b = 0.731$ (0.12) (Fig.14a and b). It is also of interest to note that in the channel, descending flows from the top wall and from the shear layer are formed above these dimples and inside them, i. e., these dimples capture the liquid from the space around them. The temperature inside the vortex core in dimples slightly changes, but its level for the conical dimple much exceeds the levels for the oval dimple of width $b = 0.731$ and the spherical dimple.

Upon the flow restructuring in the oval dimple with the insert of length $L = 1$, as the width is decreased, the positive longitudinal velocity $u_{1/2}$ grows; at that, for $L = 2$ it has a maximum local value of the order of 0.3 that is substantially higher than the same maximum value equal to 0.1 when the insert length is close to $L = 1.75$. It is worthy to note the change in the deformation of the profile of $u_{1/2}(y)$ in the flow core in the narrow channel that is most noticeable for $L = 1.75$ (curve 6) with its strong deviation from the profile of $u_{1/2}(y)$ in the plane-parallel channel. However, the profile of $u_{1/2}(y)$ for $L = 2$ also differs from other S-shaped profile inside the dimple and in particular in its strongly marked minimum local value equal to 0.08.

As the oval dimple width is decreased, the descending flow is changed to the ascending one (Fig. 14c); at that, the largest maximum value of $v_{1/2}$ equal to 0.21 is attained inside the dimple of length $L = 1.5$ and then it pretty quickly falls to 0.09 at $L = 2$.

As the oval dimple width is decreased from 0.731 to 0.429 (Fig. 14d), the minimum value of the transverse velocity component $w_{1/2}$ gradually grows in absolute magnitude and its coordinate is shifted from the dimple bottom, reaching a value of 0.6 at $L = 1.5$. In what follows, the maximum local value of $w_{1/2}$ first increases to 0.15 at $L = 1$, then it decreases to 0.1 at $L = 1.5$ and is shifted to the top wall. The profile of $w_{1/2}(y)$ in the flow core is positive and close to a constant value, consequently, the velocity vector above the oval dimple oriented to the left is slightly inclined to the right. For the oval-trench dimple with the insert of length $L = 1.75$, the minimum value of $w_{1/2}$ gradually decreases in absolute magnitude, the maximum value of $w_{1/2}$ also decreases and is shifted to the top wall. The profile for the dimple with $L = 2$ qualitatively and quantitatively differs from that with $L = 1.75$. There is no inclination of the velocity vector in the flow core above the dimple. Instead of the maximum value of $w_{1/2}$, the second minimum local value appears, and the first minimum value of $w_{1/2}$ is equal to -0.25. The dynamics of the profiles of the Cartesian velocity components, when only one central dimple is considered, illustrates the fast changes in the vortex flow field in oval-trench dimples.

Such a conclusion is to a certain extent confirmed by the profiles of the temperature $T_{1/2}$ (Fig. 14e). If at $L = 1$ and 1.5 (curves 4 and 5) the temperature in the vortex flow core in the dimple decreases, then at $L = 1.75$ it starts increasing slightly and at $L = 2$ it grows in the near-wall zone, which is undoubtedly due to the changes in the profile of $w_{1/2}(y)$.

4.5. Turbulent parameter distributions

Table 2 and Fig. 15 contain the turbulent flow characteristics in the narrow channel with conical and oval dimples.

Attention is paid to a monotonic decrease in the maximum value of turbulence energy when the dimple width b is decreased. This is indicative of the fact that the vortex flow in the oval dimple has a tendency to linearization. In the case of the conical dimple, the maximum turbulence energy value appears to be higher than the similar value in the case of the spherical dimple, and the maximum value of generated vortex viscosity turns to be almost the same for the both dimples. The maximum value of vortex viscosity for oval-trench dimples decreases by a factor of more than 1.6 in comparison to symmetric dimples.

In Fig. 15, the comparison of the profiles of turbulence energy and Re-normalized vortex viscosity as a whole is consistent with the conclusions obtained on the basis of the analysis of the considered maximum characteristics.

The maximum value of turbulence energy for the spherical dimple significantly exceeds the similar maximum values for the conical dimple and the oval dimple of width $b = 0.731$ (0.055–0.035 and 0.04, respectively). After the separated flow has been restructured for the oval dimple with $L = 1$, the local minimum appears in the profile of $k_{1/2}(y)$ and the second maximum larger in magnitude is shifted to the zone above the dimple. As the oval dimple width is decreased, the second maximum gradually decreases; at $L = 1.75$ and 2 (of order 0.02) it is not too different from the maximum of $k_{1/2}$ in the plane-parallel channel (0.012).

Normalized vortex viscosity is as a whole consistent with the behavior of turbulence energy. Its maximum value for the spherical dimple far exceeds the similar maximum values for the conical dimple and the oval dimple of width $b = 0.731$ (20–13 and 16, respectively); at that, the dependences $\mathrm{Re}\nu_{t1/2}(y)$ for the conical dimple already has a second maximum along the periphery at the dimple boundary $y = 0$. As the oval dimple width is decreased, the maximum values for the conical dimple in the dependence $\mathrm{Re}\nu_{t1/2}(y)$ decrease and are substantially lower than those for the channel flow core. The normalized viscosity level near the wall at $L = 1.75$ and 2 does not exceed 5, i.e., 4 times lower in comparison to the spherical dimple.

4.6. Analysis of integral thermal-hydraulic characteristics in the channel with conical and oval dimples of variable width and fixed spot area

The assessment of the influence of the oval-dimple width b on integral characteristics of flow and heat transfer is the central objective of this study. As the width b is decreased, the dimple lengthening increases (from 1 to 6.78) and, hence, the dimple impact on flow in the near wake. The region-averaged total Nusselt number Nu_n is calculated over the 3-long and 2-wide rectangular section surrounding the dimple (shifted by 0.5 relative to the center downstream), not considering and considering the increase in the curvilinear surface of the dimple (Nu_{no}). Fig. 16 and Table 3 illustrate the ratio of the total Nusselt number Nu_n over the section (denoted by 1 in Table 3) of the dimpled wall to the equivalent characteristic Nusselt number Nu_{npl} for the plane channel. As described in [38], hydraulic losses are determined by averaging over the boundaries of the control region of the dimpled (ζ) and plane (ζ_{pl}) channels (Fig. 3). The thermal-hydraulic efficiency (THE) is calculated as the ratio of the total thermal efficiency Nu_n/Nu_{npl} over the selected section to the relative hydraulic losses ζ/ζ_{pl} at the boundaries of the section. Fig. 17 considers the integral thermal and thermal-hydraulic characteristics of the rectangular section (denoted by 2 in Table 3) surrounding the oval dimple at an angle of inclination of 45° to the incoming flow as the dimple width dependences (Fig. 3). Relative heat transfer from the dimple with regard (in brackets) and no regard (without brackets) to the dimple surface area is also analyzed.

The results on the distinctive features of integral thermal-hydraulic characteristics in the dimpled channel are summarized in Conclusions.

5. Conclusions

1. The consideration of oval dimples consisting of two halves of the spherical dimple connected by a cylindrical insert of length L and located at an angle of inclination of 45° to the incoming flow in the channel identified the lack of attention to oval-trench dimples with the length-to-width ratio of more than 3–4.

   Methodically, it was important to fix the spot area of the dimple and its depth for one and the same channel. The problem was stated for convective heat transfer in the narrow channel with the width of 2.5, the height of 0.3, and the length of approx. 7 in terms of spot diameter of the equivalent spherical dimple at the heated wall for q = const. As in the previous numerous tests, the side walls were thermally insulated, the top wall was isothermal and kept at a 'room' temperature at the channel inlet. Water served as the working medium. The Reynolds number was 10^4, and the depth of the dimple was moderate and equal to 0.13 (0.389 of the channel height). It should be emphasized that the depth of the oval dimple in terms of width was ranged from 0.13 to 0.375 (at a length increase of 6.78).

2. The methodology of solving tasks is associated with the use of original multiblock computational technologies based on simple-topology different-scale structured overlapping grids with a special region near the dimple and with a wake behind the dimple meant for solving RANS equations – steady Reynolds-averaged Navier-Stokes equations. In the present work, the multiblock computational technologies are implemented in the VP2/3 code, and the turbulence models and the boundary conditions for heat transfer are tested. The complex is debugged and the data processing is described.
3. A detailed study of fluid dynamics and heat transfer in the narrow channel with a variable-width oval dimple and a comparative analysis of 10^0-truncated conical and basic spherical dimples allowed the following conclusions to be made.
   - 3.1. The first group of dimples is selected. These dimples have similar characteristics and among them are the conical and spherical dimples and also the 0.731-wide oval dimple with the cylindrical insert of length $L = 0.5$. This group of dimples is characterized by a common separated flow zone formed on the entire inner surface of dimples. These dimples exert a substantial influence on flow in the channel and, in particular, near the opposite plane wall.
   - 3.2. Oval dimples with the insert of the length ranging from 0.625 to 0.9 are considered. In the dimples, separated flow is gradually restructured, the separated flow zone is localized behind the leading edge and backflow is augmented in it. The dimple becomes non-stagnant and separated as a whole.
   - 3.3. For the oval dimples with the insert of the length ranging from 1 to 1.5, the vortex flow undergoes restructuring with the steady position of a vortex braid leaving the dimple on the trailing edge of the dimple on the windward side.
   - 3.4. Oval-trench dimples with $L = 1.75$ and 2 are structured with two zones having different thermal efficiency: a) the inlet region of a dimple with a short separation zone and flow acceleration is characterized by powerful heat transfer both inside and behind the dimple; b) the outlet region adjacent to the trailing edge has low heat transfer

on the inner surface of the dimple and peak heat loads in the vicinity of the thin edge. For the most narrow (0.346) and long (6.78 in terms of width) dimple, the relative depth in terms of width has appeared to be largest and equal to 0.39 and the best thermal and thermal-hydraulic characteristics have been obtained. Hydraulic losses in the considered channel with this dimple slightly differ from those in the case of the basic spherical dimple.

3.5. The main advantage of oval dimples in comparison to symmetric ones lies in secondary flow augmentation in the dimple. If for the first group of dimples the maximum values of the secondary flow velocity are equal to 0.2–0.3, then for the oval-trench dimple with $L = 2$ the maximum values are 0.8.

3.6. Flow dynamics of oval-trench dimples has the following feature: the positive friction region of a long dimple (approximately the diameter of the spot area of the spherical dimple) is formed over the longitudinal middle cross section located directly behind the intense separation zone, but not covering the long dimple.

3.7. The analysis of local and integral heat transfer in the narrow channel with oval-trench dimples involving the averaging over the longitudinal and transverse strips of the chosen control region has shown that

- it is somewhat paradoxical, but in the leading edge zone of dimples, including in the intense separated flow zone, there occurs the region of low temperatures and high heat transfer in comparison to two-fold heat transfer from the plane wall practically having a constant length (0.9 of the characteristic size – the spot diameter of the spherical dimple, which is equivalent to 2.6 in terms of width of the longest dimple);
- maximum transverse strip-averaged heat transfer in this intense heat transfer region reaches a value of 1.9;
- on the windward side of the oval-trench dimple, longitudinal strip-averaged heat transfer has increased by a factor of 3 in comparison to that from the plane wall. However, the leeward side of the dimple half is characterized by an insignificant change in heat transfer (0.9–1.3); at that, the longest dimple has a narrow zone with decreasing heat transfer.

3.8. Distinctive features of integral thermal-hydraulic characteristics in the dimples channel.

3.8.1. As the oval dimple insert length equal to 6.78 (in terms of width) is increased, the thermal-hydraulic characteristics of the rectangular section of the dimpled channel are radically improved in comparison to the spherical analog: the thermal hydraulic efficiency is from 1.162 to 1.002; at that, for the latter with the consideration of increase in the streamlined wall section, the obtained thermal hydraulic efficiency is less than 1.

3.8.2. For the rectangular section with oval-trench dimples, the rate of increase in the thermal efficiency is significantly ahead of the growth of hydraulic losses. The thermal efficiency of the dimple of length $L = 2$ is 6 times higher than that of the spherical dimple with no regard to the inner surface of the dimple and is preferable 4 times with regard to the streamlined wall section ($Nu_n/Nu_{npl} = 1.243–1.063$ and 1.19–1.054, respectively).

3.8.3. Hydraulic losses over the section with the oval dimple of width of $b = 0.549$ (the cylindrical insert of length 1) have a maximum value. For the spherical dimple, this magnitude 1.5 times exceeds the value of hydraulic losses. Hydraulic losses over the section with the narrow oval-trench dimple ($L = 2$) have appeared to be lowest and only by 13% exceed hydraulic losses over the section with the basic spherical dimple.

3.8.4. The 10°-truncated conical dimple has significant thermal efficiency exceeding 2.3 times that of the spherical dimple. However, bearing in mind this, the conical dimple is 1.65 times worse than the narrow oval-trench dimple. With allowance for increase in the streamlined surface section, the conical dimple insignificantly (1.35 times) exceeds the spherical dimple, but it is even more interior to the oval-trench dimple ($L = 2$) than without regard to the inner surface – 2.9 times.

3.8.5. The comparison of the thermal efficiencies of oval and basic spherical dimples shows the 7.1-fold advantage of the narrow and long oval dimple (with allowance for increase in the inner surface section – 5.75). This is indicative of the fact that the oval dimple increases 1.98 times heat transfer from the wall in the dimple, exceeding heat transfer from the equivalent section of the plane-parallel channel (with the consideration of increase in the streamlined surface section of the dimple this value is lower – 1.48).

3.8.6. The maximum value of hydraulic losses for the area surrounding the oval-trench dimple ($L = 2$) is of the order of 1.175 and some scatter of predictions is seen after this value, but the tendency for decrease in relative hydraulic losses with decreasing dimple width is clear. It should be noted that these losses substantially exceed the similar ones for the first section with the oval dimple; these losses are 1.5 times less than those for the spherical dimple, which is substantially higher than for the first section.

3.8.7. The thermal-hydraulic efficiency of the oval-trench dimple is very high – 1.79 (1.34 with regard to the dimple surface increase). For the spherical dimple, this parameter is equal to 0.98 (0.93). The thermal-hydraulic efficiency of the conical dimple is equal to 1.07 (0.84).

In general, it can be stated that the oval-trench dimples are dramatically superior to the symmetric analogs primarily because they are more efficient vortex generators.

Acknowledgement

The authors acknowledge gratefully the support of the Government of Russia (Grant No. 14.Z50.31.003, the leading scientist – Prof. S Isaev, Kazan Scientific Research Technical University – KAI).

References

[1] G.A. Dreitser, Problems in developing highly efficient tubular heat exchangers, Therm. Eng. 53 (4) (2006) 279–287.
[2] R.L. Hagen, A.M. Danak, Heat transfer in the field of the turbulent boundary layer separation over a dimple, Heat Transfer (4) (1967) 62–69.
[3] K.H. Presser, Empirische gleichungen zur berechnung der stoff – und warmeubertragung fur den spezialfal der abgerissenen stromung, Int. J. Heat Mass Transf. 15 (1972) 2447–2471.
[4] M. Hiwada, T. Kawamura, J. Mabuchi, M. Kumada, Some characteristics of flow pattern and heat transfer past a circular cylinder cavity, Bull. JSME 26 (220) (1983) 1744–1758.
[5] S. Snedeker, D.P. Donaldson, Observation of bistable flow in hemispherical cavity, AIAA J. 4 (1966) 735–736.
[6] P.R. Gromov, A.B. Zobnin, M.I. Rabinovich, M.M. Sushchik, Creation of solitary vortices in a flow around shallow spherical depressions, Sov. Tech. Phys. Lett. 12 (11) (1986) 1323–1328.
[7] V.S. Kesarev, A.P. Kozlov, Convective heat transfer in turbulized flow past a hemispherical cavity, Heat Transfer – Sov. Res. 25 (1993) 156–160.

[8] N. Syred, A. Khalatov, A. Kozlov, A. Shchukin, R. Agachev, Effect of surface curvature on heat transfer and hydrodynamics within a single hemispherical dimple, ASME J. Turbomach. 123 (2001) 609–613.
[9] G.I. Kiknadze, I.A. Gachechiladze, A.Yu. Gorodkov, Self-organization of vortex jets in flows of gases and liquids and the technologies utilizing this phenomenon, in: Proceedings of 2009 ASME Summer Heat Transfer Conference, San Francisco, California USA, HT 2009–88644, 2009, pp. 1–14.
[10] P.M. Ligrani, M.M. Oliveira, T. Blaskovich, Comparison of heat transfer augmentation techniques, AIAA J. 41 (3) (2003) 337–362.
[11] V.N. Afanasyev, Y.P. Chudnovsky, A.I. Leontiev, P.S. Roganov, Turbulent low friction and heat transfer characteristics of spherical cavities on a plate, Exp. Thermal Fluid Sci. 7 (1993) 1–8.
[12] M.K. Chyu, Y. Yu, H. Ding, Heat transfer enhancement in rectangular channels with concavities, J. Enhan. Heat Transfer 6 (1999) 429–439.
[13] V.I. Terekhov, S.V. Kalinina, Yu.M. Mshvidobadze, Heat transfer coefficient and aerodynamic resistance on a surface with a single dimple, J. Enhan. Heat Transfer 4 (1997) 131–145.
[14] J. Turnow, Flow Structure and Heat Transfer on Dimpled Surfaces, PhD Thesis, University of Rostock, 2011.
[15] P.M. Ligrani, J.L. Harrison, G.I. Mahmmod, M.L. Hill, Flow structure due to dimple depressions on a channel surface, Phys. Fluids 13 (11) (2001) 3442–3451.
[16] G.I. Mahmood, M.Z. Sabbagh, P.M. Ligrani, Heat transfer in a channel with dimples and protrusions on opposite walls, J. Thermophys. Heat Transfer 15 (3) (2001) 275–283.
[17] P.M. Ligrani, G.I. Mahmood, J.L. Harrison, C.M. Clayton, D.I. Nelson, Flow structure and local Nusselt number variations in a channel with dimples and protrusions on opposite walls, Int. J. Heat Mass Transf. 45 (2001) 2011–2020.
[18] P.A. Baranov, S.A. Isaev, A.I. Leontiev, A.V. Mityakov, V.Yu. Mityakov, S.Z. Sapozhnikov, Experimental and numerical modeling of vortex heat transfer in turbulent flow past spherical dimple on a plane, Thermophys. Aeromech. 9 (4) (2002) 497–508.
[19] S.V. Ekkad, H. Nasir, Dimple enhanced heat transfer in high aspect ratio channels, J. Enhan. Heat Transfer 10 (4) (2003) 395–405.
[20] G.I. Mahmood, P.M. Ligrani, Heat transfer in a dimpled channel combined influences of aspect ratio, temperature, Reynolds number and flow structure, Int. J. Heat Mass Transfer 45 (2004) 2011–2020.
[21] V.Yu. Mityakov, A.V. Mityakov, S.Z. Sapozhnikov, S.A. Isaev, Local heat fluxes on the surfaces of dimples, ditches and cavities, Therm. Eng. 54 (3) (2007) 200–203.
[22] S.A. Isaev, S.Z. Sapozhnikov, V.Yu. Mityakov, A.V. Mityakov, S.A. Mozhaiskii, A. E. Usachov, Numerical analysis of the influence of the physical viscosity on the vortex heat transfer in laminar and turbulent flows around a heated plate with a shallow spherical hole, J. Eng. Phys. Thermophys. 82 (5) (2009) 847–857.
[23] A.V. Voskoboinik, V.A. Voskoboinik, S.A. Isaev, V.L. Zhdanov, N.V. Kornev, J. Turnow, Bifurcation of vortex flow inside a spherical dimple in the narrow channel, Appl. Hydromech. (4) (2011) 3–21.
[24] Ja.P. Chudnovskii, S.A. Isaev, V.B. Kharchenko, Calculation of a three-dimensional flow of a viscous incompressible liquid in the neighborhood of a shallow well on a flat surface, J. Eng. Phys. Thermophys. 67 (5–6) (1994) 1013–1017.
[25] S.A. Isaev, A.I. Leontiev, D.P. Frolov, V.B. Kharchenko, Identification of self-organizing structures by the numerical simulation of laminar three-dimensional flow around a crater around on a plane by a flow of viscous incompressible fluid, Tech. Phys. Lett. 24 (3) (1998) 209–211.
[26] S.A. Isaev, A.I. Leontiev, A.E. Usachov, Numerical study of the eddy mechanism of enhancement of heat and mass transfer near a surface with a cavity, J. Eng. Phys. Thermophys. 71 (3) (1998) 481–487.
[27] S.A. Isaev, A.I. Leontiev, P.A. Baranov, Identification of self-organized vortex structures in numerically simulated turbulent flow of a viscous incompressible liquid streaming around a well on a plane, Tech. Phys. Lett. 26 (1) (2000) 15–18.
[28] S.A. Isaev, A.I. Leontiev, P.A. Baranov, A.E. Usachov, Bifurcation of vortex turbulent flow and intensification of heat transfer in a hole, Dokl. Phys. 45 (8) (2000) 389–391.
[29] S.A. Isaev, P.A. Baranov, A.I. Leontiev, A.E. Usachov, Numerical investigation of tornado enhancement of heat and mass exchange processes in flow past projections in concave surfaces, Heat Transfer Res. 33 (1–2) (2002) 47–55.
[30] S.A. Isaev, A.I. Leontiev, Kh.T. Metov, V.B. Kharchenko, Modeling of the influence of viscosity on the tornado heat exchange in turbulent flow around a small hole on the plane, J. Eng. Phys. Thermophys. 75 (4) (2002) 890–898.
[31] S.A. Isaev, A.I. Leontiev, P.A. Baranov, I.A. Pyshnyi, Numerical analysis of the influence of the depth of a spherical hole on a plane wall on turbulent heat transfer, J. Eng. Phys. Thermophys. 76 (1) (2003) 61–69.
[32] Z. Wang, K.S. Yeo, B.C. Khoo, Numerical simulation of laminar channel flow over dimpled surface, AIAA Paper (3964) (2003) 1192–1202.
[33] S.A. Isaev, A.I. Leontiev, G.I. Kiknadze, N.A. Kudryavtsev, I.A. Gachechiladze, Comparative analysis of the vortex heat exchange in turbulent flows around a spherical hole and two-dimensional trench on plane wall, J. Eng. Phys. Thermophys. 78 (4) (2005) 749–761.
[34] S.A. Isaev, I.A. Pyshnyi, A.E. Usachov, V.B. Kharchenko, Verification of the multiblock computational technology in calculating laminar and turbulent flow around a spherical hole on a cannel wall, J. Eng. Phys. Thermophys. 75 (5) (2002) 1155–1158.
[35] S.A. Isaev, A.I. Leontiev, Numerical simulation of vortex enhancement of heat transfer under conditions of turbulent flow past a spherical dimple on the wall of a narrow channel, High Temp. 41 (5) (2003) 665–679.
[36] N. Kornev, E. Hassel, H. Herwig, S. Isaev, P. Stephan, V. Zhdanov, Enhancement of heat transfer from dimpled surfaces by the use of vortex induction, Eng. Res. (Forschung im Ingenieurwesen) 69 (2) (2005) 90–100.
[37] S.A. Isaev, A.I. Leontiev, V.L. Zhdanov, N.V. Kornev, E. Hassel, Whirlwind-like enhancement of heat transfer on dimpled reliefs, Heat Transfer Res. 39 (1) (2008) 79–90.
[38] S.A. Isaev, N.V. Kornev, A.I. Leontiev, E. Hassel, Influence of the Reynolds number and the spherical dimple depth on the turbulent heat transfer and hydraulic loss in a narrow channel, Int. J. Heat Mass Transf. 53 (1–3) (2010) 178–197.
[39] S.A. Isaev, A.I. Leontiev, A.V. Shchelchkov, M.E. Gul'tsova, Reconstruction of the vortex-jet structure of the separation turbulent flow in a spherical dimple on the wall of a narrow channel with increase in the depth of the dimple and intensification of the secondary flow in it, J. Eng. Phys. Thermophys. 88 (5) (2015) 1304–1308.
[40] S.A. Isaev, A.V. Schelchkov, A.I. Leontiev, P.A. Baranov, M.E. Gulcova, Numerical simulation of the turbulent air flow in the narrow channel with a heated wall and a spherical dimple placed on it for vortex heat transfer enhancement depending on the dimple depth, Int. J. Heat Mass Transf. 94 (2016) 426–448.
[41] Y.-L. Lin, T.I.-P. Shih, M.K. Chyu, Computations of flow and heat transfer in a channel with rows of hemispherical cavities, in: ASME Paper, 1999, 99–GT-263, pp. 1–6.
[42] S.A. Isaev, A.I. Leontiev, P.A. Baranov, I.A. Pyshnyi, A.E. Usachov, Numerical analysis of the vortex intensification in a heat transfer in a channel with a set of deep spherical dimples on one of the walls, Dokl. Phys. 47 (10) (2002) 755–757.
[43] J. Park, P.R. Desam, P.M. Ligrani, Numerical prediction of flow structure above a dimpled surface in a channel, Numer. Heat Transfer 45 (Part A) (2004) 1–20.
[44] S.Y. Won, P.M. Ligrani, Numerical predictions of flow structure and local Nusselt number rations along and above dimpled surfaces with different dimple depths in a channel, Numer. Heat Transfer 46 (Part A) (2004) 549–570.
[45] X.J. Wei, Y.K. Joshi, P.M. Ligrani, Numerical simulation of laminar flow and heat transfer inside a microchannel with one dimpled surface, J. Electron. Packag. 127 (2007) 63–70.
[46] S.D. Hwang, H.G. Kwon, H.H. Cho, Heat transfer with dimple/protrusion arrays in a rectangular duct with a low Reynolds number range, Int. J. Heat Fluid Flow 29 (4) (2008) 916–926.
[47] N. Xiao, Q. Zhang, P.M. Ligrani, R. Mongia, Thermal performance of dimpled surfaces in laminar flows, Int. J. Heat Mass Transf. 52 (7–8) (2009) 2009–2017.
[48] M. Gotovsky, S. Isaev, Heat transfer enhancement by artificial roughness at Reynolds numbers related with laminar and transitional regimes for high-viscous liquids, in: Proceedings of the 14 International Heat Transfer Conference IHTC 14, IHTC 14-22303, 2010, pp. 1–8.
[49] Z. Wang, K.S. Yeo, B.C. Khoo, DNS of low Reynolds number turbulent flows in dimpled channels, J. Turbul. 7 (37) (2006) 1–31.
[50] M.A. Elyyan, Heat Transfer Augmentation Surfaces Using Modified Dimples/Protrusions, PhD Thesis, Virginia Polytechnic Institute and State University, 2008.
[51] Y. Chen, Y.T. Chew, B.C. Khoo, Enhancement of heat transfer in turbulent channel flow over dimpled surface, Int. J. Heat Mass Transf. 55 (2012) 8100–8121.
[52] R. Banker, M. Ya Belen'kii, M.A. Gotovsky, B.S. Fokin, S.A. Isaev, Experimental and computational investigation of the hydrodynamics and heat transfer in a flat channel of variable width for smooth and intensified surfaces, Heat Transfer Res. 35 (1–2) (2004) 34–43.
[53] J. Park, P.M. Ligrani, Numerical prediction of heat transfer and fluid flow characteristics for seven different dimpled surfaces in a channel, Numer. Heat Transfer 47 (Part A) (2005) 1–24.
[54] K.-Y. Kim, J.-Y. Choi, Shape optimization of a dimpled channel to enhance turbulent heat transfer, Numer. Heat Transfer 48 (Part A) (2005) 901–915.
[55] S.A. Isaev, A.I. Leontyev, A.E. Usachov, Methodological aspects of numerical modeling of vortex structures and heat transfer in viscous turbulent flows, Appl. Energy: Russ. J. Fuel, Power Heat Syst. 34 (4) (1996) 110–117.
[56] S.A. Isaev, A.I. Leontiev, P.A. Baranov, Kh.T. Metov, A.E. Usachov, Numerical analysis of the effect of viscosity on the vortex dynamics at laminar separated flow past the dimple on a plane with allowance for its asymmetry, J. Eng. Phys. Thermophys. 74 (2) (2001) 339–346.
[57] S.A. Isaev, A.I. Leontiev, A.V. Mitjakov, I.A. Pyshnyi, Intensification of jet-vortex heat transfer in asymmetric dimples, J. Eng. Phys. Thermophys. 76 (2003) 31–34.
[58] S.A. Isaev, A.I. Leontiev, P.A. Baranov, Simulation tornado-like enhancement of heat transfer for low-velocity motion of air in a rectangular channel with cavities. Part 1: selection and justification of calculation methods, Therm. Eng. 59 (3) (2007) 193–199.
[59] S.A. Isaev, A.I. Leontiev, P.A. Baranov, Simulation of tornado-like enhancement of heat transfer for low-velocity motion of air in a rectangular channel with cavities. Part 2: results of parametric studies, Therm. Eng. 54 (8) (2007) 655–663.
[60] N. Kornev, J. Turnow, E. Hassel, S. Isaev, F.-H. Wurm, Fluid mechanics and heat transfer in a channel with spherical and oval dimples, Notes Numer. Fluid Mech. Multidisc. Des. (110/2010) (2010) 231–237.

[61] S.A. Isaev, A.I. Leontiev, Problems of simulating tornado-like heat transfer turbulent flow past a dimpled relief on a narrow channel wall, J. Eng. Phys. Thermophys. 83 (4) (2010) 783–793.
[62] J. Turnow, N. Kornev, S. Isaev, E. Hassel, Vortex mechanism of heat transfer enhancement in a channel with spherical and oval dimples, Heat Mass Transfer/Waerme- und Stoffuebertragung 47 (3) (2011) 301–311.
[63] S.A. Isaev, A.I. Leontiev, N.V. Kornev, E. Hassel, Ja P. Chudnovskii, Heat transfer intensification for laminar and turbulent flows in a narrow channel with one-row oval dimples, High Temp. 53 (3) (2015) 375–386.
[64] S.A. Isaev, A.I. Leontiev, M.E. Gul'tsova, I.A. Popov, Transformation and intensification of tornado-like flow in a narrow channel during elongation of an oval dimple with constant area, Tech. Phys. Lett. 41 (6) (2015) 606–609.
[65] F.R. Menter, M. Kuntz, R. Langtry, Ten years of industrial experience with the SST turbulence model, in: K. Hajalic, Y. Nogano, M. Tummers (Eds.), Turbulence, Heat and Mass Transfer, vol. 4, Begell House Inc., 2003, pp. 1–8.
[66] S.A. Isaev, P.A. Baranov, Yu.V. Zhukova, A.E. Usachov, V.B. Kharchenko, Correction of the shear-stress-transfer model with account for the curvature of streamlines in calculating separated flows of an incompressible viscous fluid, J. Eng. Phys. Thermophys. 87 (4) (2014) 1002–1015.
[67] S.A. Isaev, P.A. Baranov, A.E. Usachov, Multiblock Computational Technologies in the VP2/3 Package on Aerothermodynamics, LAP LAMBERT Academic Publishing, Saarbrucken, 2013, pp. 1–316.
[68] J.P. Van Doormaal, G.D. Raithby, Enhancement of the SIMPLE method for predicting incompressible fluid flow, Numer. Heat Transfer 7 (2) (1984) 147–163.
[69] C.M. Rhie, W.L. Chow, A numerical study of the turbulent flow past an isolated airfoil with trailing edge separation, AIAA J. 21 (1983) 1525–1532.
[70] A. Pascau, N. Garcia, Consistency of SIMPLEC scheme in collocated grids, in: Proceedings of V European Conference on Computational Fluid Dynamics ECCOMAS CFD 2010, Lisbon, Portugal, 2010, pp. 1–12.
[71] B.P. Leonard, A stable and accurate convective modeling procedure based on quadratic upstream interpolation, J. Comput. Meth. Appl. Mech. Eng. 19 (1) (1979) 59–98.
[72] B. Van Leer, Towards the ultimate conservative difference scheme. V. A second order sequel to Godunov's method, J. Comput. Phys. 32 (1979) 101–136.
[73] Y. Saad, Iterative Methods for Sparse Linear Systems, second ed., Society for Industrial and Applied Mathematics, Philadelphia, 2003, pp. 1–567.
[74] D. Demidov, AMGCL: C++ Library for Solving Large Sparse Linear Systems with Algebraic Multigrid Method, 2012 <http://amgcl.readthedocs.org/>.
[75] S.A. Isaev, V.L. Zhdanov, H.-J. Niemann, Numerical study of the bleeding effect on the aerodynamic characteristics of a circular cylinder, J. Wind Eng. Ind. Aerodyn. 90 (11) (2002) 1217–1226.
[76] S.A. Isaev, A.G. Sudakov, P.A. Baranov, Yu.V. Zhukova, A.E. Usachov, Analysis of errors of multiblock computational technologies by the example of calculating a circulation flow in a square cavity with a moving cover at Re = 1000, J. Eng. Phys. Thermophys. 86 (5) (2013) 1134–1150.
[77] Y. Zheng, M.-S. Liou, A novel approach of three-dimensional hybrid grid methodology: part 1, grid generation, J. Comput. Meth. Appl. Mech. Eng. 192 (2003) 4147–4171.